Available online at www.sciencedirect.com
SCIENCE DIRECT®
International Journal of Solids and Structures 43 (2006) 1638–1668
INTERNATIONAL JOURNAL OF SOLIDS and STRUCTURES
www.elsevier.com/locate/ijsolstr

Loosening of elastic inclusions

S.L. Crouch *, S.G. Mogilevskaya

Department of Civil Engineering, University of Minnesota, 500 Pillsbury Drive S.E., Minneapolis, Minnesota 55455, USA

Received 26 November 2004; received in revised form 15 March 2005
Available online 21 April 2005

Abstract

A numerical method is presented for simulating the occurrence of localized slip and separation along the interfaces of multiple, randomly distributed, circular elastic inclusions in an infinite elastic plane. The method is an extension of a direct boundary integral approach previously described elsewhere for solving problems involving perfectly bonded circular inclusions. Here, we allow displacement discontinuities to develop along the inclusion/matrix interfaces in accordance with a linear Mohr–Coulomb yield condition combined with a tensile strength cut-off. The displacements, tractions, and displacement discontinuities on the inclusion boundaries are all represented by truncated Fourier series, and an explicit iterative algorithm is adopted to determine zones of slip and separation under the prevailing loading conditions. Several examples are given to demonstrate the accuracy and generality of the approach.

Keywords: Direct boundary integral method; Somigliana's formula; Multiple circular inclusions; Imperfect interface; Displacement discontinuities; Mohr–Coulomb yield condition; Cohesive crack model; Gibbs phenomenon; Under-relaxation

1. Introduction

In a previous paper (Crouch and Mogilevskaya, 2003) we introduced a specialized version of the direct boundary integral method for solving elasticity problems for an infinite plane containing an arbitrary number of randomly distributed circular inclusions. The numerical procedure is based on the two-dimensional version of Somigliana's formula with the boundary displacements and tractions represented by truncated Fourier series. In order to explain the method in its simplest form, we assumed that the inclusions were perfectly bonded to the surrounding material matrix. In the present paper we relax this assumption and allow for the possible occurrence of localized slip and separation along the inclusion/matrix interfaces.

* Corresponding author. Tel.: +1 612 624 6355; fax: +1 612 624 2841.
E-mail address: crouch@it.umn.edu (S.L. Crouch).

0020-7683/$ - see front matter © 2005 Elsevier Ltd. All rights reserved.
doi:10.1016/j.ijsolstr.2005.03.050

The term *imperfect interface* is used to describe a situation in which the displacements are discontinuous at the interface between an inclusion and the material matrix. The simplest model of an imperfect interface—the spring-type interface—assumes that the normal and shear components of displacement discontinuity are directly proportional to the corresponding components of traction (see, for example, Benveniste, 1985; Aboudi, 1987; Achenbach and Zhu, 1989, 1990; Hashin, 1990, 1991; Zhu and Achenbach, 1991; Sudak et al., 1999; Mogilevskaya and Crouch, 2002). The proportionality coefficients for a spring-type interface are either assumed to be constant along the periphery of the inclusion (a so-called homogeneously imperfect interface) or to vary in some manner along it (an inhomogeneously imperfect interface). In both cases it is assumed that relative deformation between the inclusion and the material matrix can be represented by the deformation of a negligibly thin layer of unconnected linear springs.

A spring-type interface model is often adopted for analyses of inclusion problems using analytical techniques (e.g. Gao, 1995; Ru, 1998) and boundary element methods (e.g. Achenbach and Zhu, 1989, 1990; Zhu and Achenbach, 1991), but this simple model has limitations. For instance, a spring-type model cannot provide any information about the displacement and stress fields within the interphase region between an inclusion and the surrounding material matrix, because the model neglects the thickness of this region. In addition, the spring-type model may permit a physically unrealistic overlapping of the inclusion/matrix interfaces to occur under some loading conditions.

More elaborate representations of inclusion/matrix interactions are possible, including finite element (Nassehi et al., 1993; Lagache et al., 1994; Al-Ostaz and Jasiuk, 1996; Wacker et al., 1998) and boundary element (Liu et al., 2000; Mogilevskaya and Crouch, 2003) models that explictly account for the presence of perfectly bonded interphases with non-zero thicknesses. Except for our own work (Mogilevskaya and Crouch, 2003), however, these approaches all assume a doubly periodic array of inclusions based on the concept of a unit cell. Our Galerkin boundary integral method allows for a random assortment of elastic inclusions and interphases, subject only to the condition that each inclusion must be concentric with the interphase that contains it. In our method, unlike other numerical approaches, the thicknesses of the interphases can be arbitrarily small. The method accurately represents both soft and stiff interphases, as classified by Benveniste and Miloh (2001).

Another important imperfect interface condition is one for which localized slip and separation occur between an inclusion and the surrounding material matrix. Comparatively little work has been reported on this topic. Stippes et al. (1962) solved the problem of debonding of a smooth circular inclusion in an infinite plate made of the same material, under uniaxial tension at infinity. Subsequently, Hussain and Pu (1971) generalized this solution for the case that the inclusion is rough so that some parts of its interface might neither slip nor separate (a condition called ''rigid linkage'' by the authors). Toya (1974) considered the problem of a traction-free, arc-shaped crack along the interface of a circular inclusion in an infinite plane and derived a debonding criterion for the interface using the principle of virtual work and Griffith's criterion. All of these analyses are for a single inclusion and the results cannot be applied to closely spaced, multiple inclusions. The boundary element models described by Achenbach and Zhu (1989, 1990) and Zhu and Achenbach (1991) contain interface cracks, but the locations of the cracks are specified a priori, and the use of a unit cell representation means that every inclusion in the doubly periodic array has exactly the same crack geometry, a circumstance that is unlikely to occur in reality. A noteworthy feature of Achenbach and Zhu's work, however, is that they used an iterative equation-solving technique to prohibit the occurrence of overlapping of the inclusion/matrix interfaces.

Zhao and Weng (1997), Ju and Lee (2001), and Sun et al. (2003) use a simple technique based on the concept of fictitious inclusions to indirectly simulate interface debonding. Their technique assumes that a partially debonded, isotropic elastic inclusion can be represented by a perfectly bonded, anisotropic inclusion with its elastic constants chosen such that the principal stress in one direction is zero. These authors are concerned with approximating effective material properties and assume that the detailed displacement and stress fields can be ignored for this purpose. They also assume that interactions among multiple inclusions

can be neglected when evaluating the effective material properties, and that localized debonding does not alter the principal stress directions in and around the inclusions (Sun et al., 2003). The authors acknowledge that the latter assumption is open to question.

In this paper we develop a numerical procedure for simulating the occurrence of localized slip and separation along the interfaces of multiple, randomly distributed circular elastic inclusions in an infinite elastic plane. In order to limit the number of parameters appearing in the analysis we suppose that the inclusions are perfectly bonded to the material matrix unless slip or separation takes place. We assume that interface failure is governed by a Mohr–Coulomb yield condition with a tensile strength cut-off, which is incorporated in the analysis by means of an iterative technique. Overlapping of the inclusion/matrix interfaces is prevented during the iterative equation-solving process, as in the work of Achenbach and Zhu (1989, 1990). Several examples are given to demonstrate the accuracy and utility of the general numerical approach.

2. Terminology

We consider an infinite elastic plane with Poisson's ratio ν and shear modulus μ containing K randomly distributed, non-overlapping, circular inclusions, possibly of different sizes and possibly with different elastic properties. The kth inclusion is centered at the point $(x,y)=(x_k,y_k)$ and has radius R_k and elastic constants ν_k and μ_k, as depicted in Fig. 1. The stresses at infinity are σ_{xx}^{∞}, σ_{yy}^{∞}, and σ_{xy}^{∞}.

Each inclusion can be regarded as a circular disc inserted into a circular hole of the same radius, and the boundary parameters for the discs and holes can be represented by truncated Fourier series. The boundary displacements for the kth hole, for example, can be written as

$$\begin{aligned} u_x(R_k,\theta_k) &= \frac{1}{4\mu}[k_1\sigma_{xx}^{\infty}-(1-k_2)\sigma_{yy}^{\infty}](x_k+R_k\cos\theta_k)+\frac{1}{2\mu}\sigma_{xy}^{\infty}(y_k+R_k\sin\theta_k) \\ &\quad +\frac{1}{2}a_{0k}(u_x)+\sum_{n=1}^{N_k}[a_{nk}(u_x)\cos n\theta_k+b_{nk}(u_x)\sin n\theta_k] \\ u_y(R_k,\theta_k) &= \frac{1}{2\mu}\sigma_{xy}^{\infty}(x_k+R_k\cos\theta_k)+\frac{1}{4\mu}[-(1-k_2)\sigma_{xx}^{\infty}+k_1\sigma_{yy}^{\infty}](y_k+R_k\sin\theta_k) \\ &\quad +\frac{1}{2}a_{0k}(u_y)+\sum_{n=1}^{N_k}[a_{nk}(u_y)\cos n\theta_k+b_{nk}(u_y)\sin n\theta_k] \end{aligned} \tag{1}$$

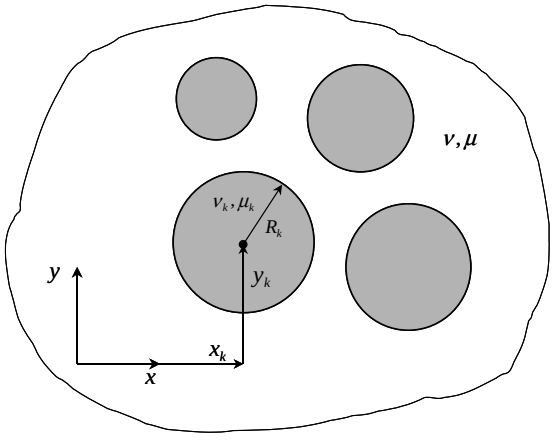

Fig. 1. Multiple circular inclusions in an infinite plane.

where θ_k is the local polar angle relative to the center of the hole (see Fig. 1), N_k is the number of terms in the Fourier series (N_k may be different for each hole), and constants k_1 and k_2 are defined as follows:

$$k_1 = 2(1-\nu); \quad k_2 = 1-2\nu \tag{2}$$

The first groups of terms in (1) give the displacements in a plane without any holes due to the stresses at infinity. (We assume plane strain conditions.) These "initial" displacements are measured relative to a fixed reference point at the origin. The other terms in (1) represent the changes in displacement due to the presence of the holes. The notation $a_{nk}(u_x)$, $b_{nk}(u_x)$ and $a_{nk}(u_y)$, $b_{nk}(u_y)$ is used to differentiate between the Fourier coefficients for the two components of displacement; no functional dependence on u_x and u_y is implied.

The tractions for the kth hole can similarly be written as the sums of the initial tractions and the changes due to the presence of the holes:

$$\begin{aligned} t_x(R_k,\theta_k) &= -(\sigma^\infty_{xx}\cos\theta_k + \sigma^\infty_{xy}\sin\theta_k) + \sum_{n=1}^{N_k}[a_{nk}(t_x)\cos n\theta_k + b_{nk}(t_x)\sin n\theta_k] \\ t_y(R_k,\theta_k) &= -(\sigma^\infty_{xy}\cos\theta_k + \sigma^\infty_{yy}\sin\theta_k) + \sum_{n=1}^{N_k}[a_{nk}(t_y)\cos n\theta_k + b_{nk}(t_y)\sin n\theta_k] \end{aligned} \tag{3}$$

The minus signs are needed for the initial tractions because the components of the unit outward normal to the boundary of the hole are negative: $(n_x, n_y) = (-\cos\theta_k, -\sin\theta_k)$. Also, the $n = 0$ terms of the Fourier expansions for the tractions are set equal to zero in order for the resultant force to vanish for every hole. It can be shown (Crouch and Mogilevskaya, 2003) that vanishing of the resultant moment on each hole requires that $a_{1k}(t_y) = b_{1k}(t_x)$ for $k = 1$ to K. Again, the notation $a_{nk}(t_x)$, $b_{nk}(t_x)$ and $a_{nk}(t_y)$, $b_{nk}(t_y)$ is used merely to differentiate between the Fourier coefficients for the two components of traction and does not signify a functional dependence on t_x and t_y.

In the same manner, the boundary displacements for the kth disc (inclusion) can be represented as

$$\begin{aligned} u'_x(R_k,\theta_k) &= \frac{1}{4\mu_k}[k_{1k}\sigma^\infty_{xx} - (1-k_{2k})\sigma^\infty_{yy}](x_k + R_k\cos\theta_k) + \frac{1}{2\mu_k}\sigma^\infty_{xy}(y_k + R_k\sin\theta_k) \\ &\quad + \frac{1}{2}a'_{0k}(u_x) + \sum_{n=1}^{N_k}[a'_{nk}(u_x)\cos n\theta_k + b'_{nk}(u_x)\sin n\theta_k] \\ u'_y(R_k,\theta_k) &= \frac{1}{2\mu_k}\sigma^\infty_{xy}(x_k + R_k\cos\theta_k) + \frac{1}{4\mu_k}[-(1-k_{2k})\sigma^\infty_{xx} + k_{1k}\sigma^\infty_{yy}](y_k + R_k\sin\theta_k) \\ &\quad + \frac{1}{2}a'_{0k}(u_y) + \sum_{n=1}^{N_k}[a'_{nk}(u_y)\cos n\theta_k + b'_{nk}(u_y)\sin n\theta_k] \end{aligned} \tag{4}$$

in which

$$k_{1k} = 2(1-\nu_k); \quad k_{2k} = 1-2\nu_k \tag{5}$$

and where the prime ($'$) is used here and in the sequel to identify quantities associated with the inclusions. The corresponding tractions are

$$\begin{aligned} t'_x(R_k,\theta_k) &= \sigma^\infty_{xx}\cos\theta_k + \sigma^\infty_{xy}\sin\theta_k + \sum_{n=1}^{N_k}[a'_{nk}(t_x)\cos n\theta_k + b'_{nk}(t_x)\sin n\theta_k] \\ t'_y(R_k,\theta_k) &= \sigma^\infty_{xy}\cos\theta_k + \sigma^\infty_{yy}\sin\theta_k + \sum_{n=1}^{N_k}[a'_{nk}(t_y)\cos n\theta_k + b'_{nk}(t_y)\sin n\theta_k] \end{aligned} \tag{6}$$

where moment equilibrium again gives $a'_{1k}(t_y) = b'_{1k}(t_x)$ for $k = 1$ to K. The initial displacements and stresses are included in (4) and (6) for conformity with (1) and (3); these terms would not be required if we were considering a boundary value problem for an isolated disc.

Equilibrium along the boundaries of the inclusions requires that

$$\begin{aligned} t_x(R_k,\theta_k) + t'_x(R_k,\theta_k) &= 0 \\ t_y(R_k,\theta_k) + t'_y(R_k,\theta_k) &= 0 \end{aligned} \tag{7}$$

for $-\pi \leqslant \theta_k \leqslant \pi$ and $k = 1$ to K, and it follows from (3) and (6) that

$$\begin{aligned} a'_{nk}(t_x) &= -a_{nk}(t_x); \quad b'_{nk}(t_x) = -b_{nk}(t_x) \\ a'_{nk}(t_y) &= -a_{nk}(t_y); \quad b'_{nk}(t_y) = -b_{nk}(t_y) \end{aligned} \tag{8}$$

for $n = 1$ to N_k. We note for future reference that these conditions also hold in the event that localized separation (cracking) occurs over a part of an interface; in this case the tractions $t_x(R_k,\theta_k)$, $t_y(R_k,\theta_k)$ and $t'_x(R_k,\theta_k), t'_y(R_k,\theta_k)$ are individually equal to zero for those values of θ_k that define the zone(s) of separation.

In view of (8), we may rewrite (6) to express the tractions on the boundary of the inclusion in terms of the Fourier coefficients for the tractions on the boundary of the hole into which it is fitted:

$$\begin{aligned} t'_x(R_k,\theta_k) &= \sigma^\infty_{xx}\cos\theta_k + \sigma^\infty_{xy}\sin\theta_k - \sum_{n=1}^{N_k}[a_{nk}(t_x)\cos n\theta_k + b_{nk}(t_x)\sin n\theta_k] \\ t'_y(R_k,\theta_k) &= \sigma^\infty_{xy}\cos\theta_k + \sigma^\infty_{yy}\sin\theta_k - \sum_{n=1}^{N_k}[a_{nk}(t_y)\cos n\theta_k + b_{nk}(t_y)\sin n\theta_k] \end{aligned} \tag{9}$$

This measure allows us to reduce the number of Fourier coefficients appearing in the analysis.

The components of displacement discontinuity for the kth inclusion are defined as the differences between the boundary displacements of the hole and disc as follows:

$$\begin{aligned} \Delta u_x(R_k,\theta_k) &= u_x(R_k,\theta_k) - u'_x(R_k,\theta_k) \\ \Delta u_y(R_k,\theta_k) &= u_y(R_k,\theta_k) - u'_y(R_k,\theta_k) \end{aligned} \tag{10}$$

i.e.

$$\begin{aligned} \Delta u_x(R_k,\theta_k) &= \frac{1}{2}(\alpha_{2k}\sigma^\infty_{xx} - \alpha_{3k}\sigma^\infty_{yy})(x_k + R_k\cos\theta_k) + \alpha_{1k}\sigma^\infty_{xy}(y_k + R_k\sin\theta_k) \\ &\quad + \frac{1}{2}(a_{0k}(u_x) - a'_{0k}(u_x)) + \sum_{n=1}^{N_k}\Big[(a_{nk}(u_x) - a'_{nk}(u_x))\cos n\theta_k + (b_{nk}(u_x) - b'_{nk}(u_x))\sin n\theta_k\Big] \\ \Delta u_y(R_k,\theta_k) &= \frac{1}{2}(-\alpha_{3k}\sigma^\infty_{xx} + \alpha_{2k}\sigma^\infty_{yy})(y_k + R_k\sin\theta_k) + \alpha_{1k}\sigma^\infty_{xy}(x_k + R_k\cos\theta_k) \\ &\quad + \frac{1}{2}(a_{0k}(u_y) - a'_{0k}(u_y)) + \sum_{n=1}^{N_k}\Big[(a_{nk}(u_y) - a'_{nk}(u_y))\cos n\theta_k + (b_{nk}(u_y) - b'_{nk}(u_y))\sin n\theta_k\Big] \end{aligned} \tag{11}$$

in which we have set

$$\begin{aligned}\alpha_{1k} &= \frac{1}{2\mu} - \frac{1}{2\mu_k} \\ \alpha_{2k} &= \frac{k_1}{2\mu} - \frac{k_{1k}}{2\mu_k} \\ \alpha_{3k} &= \frac{1-k_2}{2\mu} - \frac{1-k_{2k}}{2\mu_k}\end{aligned} \tag{12}$$

The left-hand sides of (11) can also be represented by truncated Fourier series:

$$\begin{aligned}\Delta u_x(R_k,\theta_k) &= \frac{1}{2}a_{0k}(\Delta u_x) + \sum_{n=1}^{N_k}[a_{nk}(\Delta u_x)\cos n\theta_k + b_{nk}(\Delta u_x)\sin n\theta_k] \\ \Delta u_y(R_k,\theta_k) &= \frac{1}{2}a_{0k}(\Delta u_y) + \sum_{n=1}^{N_k}[a_{nk}(\Delta u_y)\cos n\theta_k + b_{nk}(\Delta u_y)\sin n\theta_k]\end{aligned} \tag{13}$$

For a perfectly bonded inclusion the displacement discontinuities are zero, i.e. $\Delta u_x(R_k,\theta_k) = \Delta u_y(R_k,\theta_k) = 0$, in which case the Fourier coefficients $a_{0k}(\Delta u_x)$, $a_{nk}(\Delta u_x)$, $b_{nk}(\Delta u_x)$, etc. in (13) are all equal to zero.

By direct comparison of (11) and (13) we find the following expressions for the Fourier coefficients for the displacement discontinuities:

(1) For $n = 0$

$$\begin{aligned}a_{0k}(\Delta u_x) &= a_{0k}(u_x) - a'_{0k}(u_x) + (\alpha_{2k}\sigma^\infty_{xx} - \alpha_{3k}\sigma^\infty_{yy})x_k + 2\alpha_{1k}\sigma^\infty_{xy}y_k \\ a_{0k}(\Delta u_y) &= a_{0k}(u_y) - a'_{0k}(u_y) + 2\alpha_{1k}\sigma^\infty_{xy}x_k + (-\alpha_{3k}\sigma^\infty_{xx} + \alpha_{2k}\sigma^\infty_{yy})y_k\end{aligned} \tag{14}$$

(2) For $n = 1$

$$\begin{aligned}a_{1k}(\Delta u_x) &= a_{1k}(u_x) - a'_{1k}(u_x) + \frac{1}{2}(\alpha_{2k}\sigma^\infty_{xx} - \alpha_{3k}\sigma^\infty_{yy})R_k \\ b_{1k}(\Delta u_x) &= b_{1k}(u_x) - b'_{1k}(u_x) + \alpha_{1k}\sigma^\infty_{xy}R_k \\ a_{1k}(\Delta u_y) &= a_{1k}(u_y) - a'_{1k}(u_y) + \alpha_{1k}\sigma^\infty_{xy}R_k \\ b_{1k}(\Delta u_y) &= b_{1k}(u_y) - b'_{1k}(u_y) + \frac{1}{2}(-\alpha_{3k}\sigma^\infty_{xx} + \alpha_{2k}\sigma^\infty_{yy})R_k\end{aligned} \tag{15}$$

(3) For $n > 1$

$$\begin{aligned}a_{nk}(\Delta u_x) &= a_{nk}(u_x) - a'_{nk}(u_x) \\ b_{nk}(\Delta u_x) &= b_{nk}(u_x) - b'_{nk}(u_x) \\ a_{nk}(\Delta u_y) &= a_{nk}(u_y) - a'_{nk}(u_y) \\ b_{nk}(\Delta u_y) &= b_{nk}(u_y) - b'_{nk}(u_y)\end{aligned} \tag{16}$$

3. Basic formulae

Expressions for the displacements and stresses at points $(x,y) = (\xi_x,\xi_y)$ in both the material matrix and the inclusions are given in Appendices A and B. These results were derived by substituting the preceding

Fourier series representations for the boundary displacement and traction *changes* into the plane strain version of Somigliana's formula and carrying out all the integrations analytically (Crouch and Mogilevskaya, 2003).

In order to calculate the displacements and stresses using the formulas in the appendices, it is first necessary to know the Fourier coefficients for the boundary displacements and tractions for all of the inclusions. These quantities are determined by solving a system of algebraic equations, which is in turn based on a set of relationships connecting the Fourier coefficients for the displacements to those for the tractions. The required relationships are summarized below.

3.1. Displacement coefficients for multiple holes

Relationships between the Fourier coefficients for the displacements and tractions for a typical hole j are obtained by letting point (ξ_x, ξ_y) lie on the boundary of the hole (i.e. by taking $\xi_x = x_j + R_j \cos\theta_j$ and $\xi_y = y_j + R_j \sin\theta_j$), setting $\chi_j = \theta_j$ and $\rho_j = 1$ in Eq. (A.1), and using the definitions of the Fourier coefficients (Churchill, 1963), which, in the present notation, are

$$\begin{aligned} a_{mj}(u_x) &= \frac{1}{\pi}\int_{-\pi}^{\pi} u_x(\xi_x,\xi_y)\cos m\theta_j \,\mathrm{d}\theta_j; \quad b_{mj}(u_x) = \frac{1}{\pi}\int_{-\pi}^{\pi} u_x(\xi_x,\xi_y)\sin m\theta_j \,\mathrm{d}\theta_j \\ a_{mj}(u_y) &= \frac{1}{\pi}\int_{-\pi}^{\pi} u_y(\xi_x,\xi_y)\cos m\theta_j \,\mathrm{d}\theta_j; \quad b_{mj}(u_y) = \frac{1}{\pi}\int_{-\pi}^{\pi} u_y(\xi_x,\xi_y)\sin m\theta_j \,\mathrm{d}\theta_j \end{aligned} \tag{17}$$

After evaluating the indicated integrals and letting m equal n for notational convenience, we obtain the following results:

(1) For $n = 1$

$$\begin{aligned} a_{1j}(u_x) &= \frac{R_j}{2\mu}\left[k_1 a_{1j}(t_x) - k_2 b_{1j}(t_y)\right] + \frac{k_1}{2k_2}\left[k_3 A_{1j}(u_x) + (1-2k_2)B_{1j}(u_y)\right] \\ b_{1j}(u_x) &= \frac{R_j}{2\mu}\left[k_2 a_{1j}(t_y) + k_1 b_{1j}(t_x)\right] + \frac{1}{2}\left[k_3 A_{1j}(u_y) + (1+2k_1)B_{1j}(u_x)\right] \\ a_{1j}(u_y) &= \frac{R_j}{2\mu}\left[k_1 a_{1j}(t_y) + k_2 b_{1j}(t_x)\right] + \frac{1}{2}\left[(1+2k_1)A_{1j}(u_y) + k_3 B_{1j}(u_x)\right] \\ b_{1j}(u_y) &= \frac{R_j}{2\mu}\left[-k_2 a_{1j}(t_x) + k_1 b_{1j}(t_y)\right] + \frac{k_1}{2k_2}\left[(1-2k_2)A_{1j}(u_x) + k_3 B_{1j}(u_y)\right] \end{aligned} \tag{18}$$

(2) For $n > 1$

$$\begin{aligned} a_{nj}(u_x) &= \frac{R_j}{2\mu n}\left[k_1 a_{nj}(t_x) - k_2 b_{nj}(t_y)\right] + \frac{2k_1}{k_3}\left[k_1 A_{nj}(u_x) - k_2 B_{nj}(u_y)\right] \\ b_{nj}(u_x) &= \frac{R_j}{2\mu n}\left[k_2 a_{nj}(t_y) + k_1 b_{nj}(t_x)\right] + \frac{2k_1}{k_3}\left[k_2 A_{nj}(u_y) + k_1 B_{nj}(u_x)\right] \\ a_{nj}(u_y) &= \frac{R_j}{2\mu n}\left[k_1 a_{nj}(t_y) + k_2 b_{nj}(t_x)\right] + \frac{2k_1}{k_3}\left[k_1 A_{nj}(u_y) + k_2 B_{nj}(u_x)\right] \\ b_{nj}(u_y) &= \frac{R_j}{2\mu n}\left[-k_2 a_{nj}(t_x) + k_1 b_{nj}(t_y)\right] + \frac{2k_1}{k_3}\left[-k_2 A_{nj}(u_x) + k_1 B_{nj}(u_y)\right] \end{aligned} \tag{19}$$

in which the constant k_3 is defined as

$$k_3 = k_1 + k_2 = 3 - 4\nu \tag{20}$$

The quantities $A_{nj}(u_x)$, etc. in (18) and (19) are the Fourier coefficients for the displacements of the boundary of the jth hole due to the influences of the other $K-1$ holes, $k=1$ to K, $k \neq j$. These quantities are obtained by evaluating the following expressions (cf. (17)) and then setting m equal to n:

$$\begin{aligned} A_{mj}(u_x) &= \frac{1}{\pi}\int_{-\pi}^{\pi}\sum_{\substack{k=1\\k\neq j}}^{K} u_x(\xi_x,\xi_y)\cos m\theta_j \,\mathrm{d}\theta_j; \quad B_{mj}(u_x) = \frac{1}{\pi}\int_{-\pi}^{\pi}\sum_{\substack{k=1\\k\neq j}}^{K} u_x(\xi_x,\xi_y)\sin m\theta_j \,\mathrm{d}\theta_j \\ A_{mj}(u_y) &= \frac{1}{\pi}\int_{-\pi}^{\pi}\sum_{\substack{k=1\\k\neq j}}^{K} u_y(\xi_x,\xi_y)\cos m\theta_j \,\mathrm{d}\theta_j; \quad B_{mj}(u_y) = \frac{1}{\pi}\int_{-\pi}^{\pi}\sum_{\substack{k=1\\k\neq j}}^{K} u_y(\xi_x,\xi_y)\sin m\theta_j \,\mathrm{d}\theta_j \end{aligned} \tag{21}$$

The displacements in the integrands of these expressions are functions of the angles χ_k and dimensionless distances ρ_k from the center of the kth inclusion to points on the boundary of the jth hole. The integrals can all be evaluated analytically using integration formulas given by Crouch and Mogilevskaya (2003).

The $n=0$ coefficients $a_{0j}(u_x)$ and $a_{0j}(u_y)$ are determined by noting that expressions (A.1) and (1) are equivalent for a point on the boundary of the jth hole. Evaluation of these expressions for a single point on the boundary of each hole is sufficient to calculate the values of $a_{0j}(u_x)$ and $a_{0j}(u_y)$ (Crouch and Mogilevskaya, 2003).

3.2. Displacement coefficients for a disc

Similar relationships between the Fourier coefficients for the displacements and tractions for the jth disc (inclusion) can be written as follows:

(1) For $n=1$

$$\begin{aligned} a'_{1j}(u_x) &= -\frac{R_j}{4\mu_j}[k_{1j}a_{1j}(t_x) - (1-k_{2j})b_{1j}(t_y)] \\ b'_{1j}(u_x) &= -\frac{R_j}{2\mu_j}b_{1j}(t_x) - \frac{1}{2\pi R_j}\Omega'_j \\ a'_{1j}(u_y) &= -\frac{R_j}{2\mu_j}a_{1j}(t_y) + \frac{1}{2\pi R_j}\Omega'_j \\ b'_{1j}(u_y) &= -\frac{R_j}{4\mu_j}[-(1-k_{2j})a_{1j}(t_x) + k_{1j}b_{1j}(t_y)] \end{aligned} \tag{22}$$

where Ω'_j is the rotation of the disc, defined as

$$\Omega'_j = \int_{-\pi}^{\pi} u'_\theta(R_j,\theta_j)R_j \,\mathrm{d}\theta_j = \int_{-\pi}^{\pi}[-u'_x(R_j,\theta_j)\sin\theta_j + u'_y(R_j,\theta_j)\cos\theta_j]R_j \,\mathrm{d}\theta_j = \pi R_j[a'_{1j}(u_y) - b'_{1j}(u_x)] \tag{23}$$

Using the definitions $a_{1j}(\Delta u_y) = a_{1j}(u_y) - a'_{1j}(u_y)$ and $b_{1j}(\Delta u_x) = b_{1j}(u_x) - b'_{1j}(u_x)$ and (18) we find that

$$\Omega'_j = \pi R_j[A_{1j}(u_y) - B_{1j}(u_x)] - \pi R_j[a_{1j}(\Delta u_y) - b_{1j}(\Delta u_x)] \tag{24}$$

If the inclusion is perfectly bonded to the material matrix its rotation is due solely to the influences of the *other* $K-1$ inclusions.

(2) For $n > 1$

$$\begin{aligned}
a'_{nj}(u_x) &= -\frac{R_j}{2\mu_j n}[k_{1j}a_{nj}(t_x) + k_{2j}b_{nj}(t_y)] \\
b'_{nj}(u_x) &= -\frac{R_j}{2\mu_j n}[-k_{2j}a_{nj}(t_y) + k_{1j}b_{nj}(t_x)] \\
a'_{nj}(u_y) &= -\frac{R_j}{2\mu_j n}[k_{1j}a_{nj}(t_y) - k_{2j}b_{nj}(t_x)] \\
b'_{nj}(u_y) &= -\frac{R_j}{2\mu_j n}[k_{2j}a_{nj}(t_x) + k_{1j}b_{nj}(t_y)]
\end{aligned} \tag{25}$$

We note that relations (8) have been used to express (22) and (25) in terms of the Fourier coefficients for the tractions on the wall of the jth hole.

The values of the $n = 0$ terms $a'_{0j}(u_x)$ and $a'_{0j}(u_y)$ are obtained directly from (14):

$$\begin{aligned}
a'_{0k}(u_x) &= a_{0k}(u_x) + (\alpha_{2k}\sigma^{\infty}_{xx} - \alpha_{3k}\sigma^{\infty}_{yy})x_k + 2\alpha_{1k}\sigma^{\infty}_{xy}y_k - a_{0k}(\Delta u_x) \\
a'_{0k}(u_y) &= a_{0k}(u_y) + 2\alpha_{1k}\sigma^{\infty}_{xy}x_k + (-\alpha_{3k}\sigma^{\infty}_{xx} + \alpha_{2k}\sigma^{\infty}_{yy})y_k - a_{0k}(\Delta u_y)
\end{aligned} \tag{26}$$

3.3. Traction coefficients for multiple inclusions

The Fourier coefficients for the tractions exerted on the wall of the jth hole by the jth inclusion are found by substituting (18) and (19) and (22), (24), and (25) into (11) to eliminate reference to the displacement coefficients $a_{nj}(u_x)$, $a'_{nj}(u_x)$, etc.; setting the resulting expressions equal to (13); equating the terms involving $\sin n\theta_j$ and $\cos n\theta_j$; and then solving for $a_{nj}(t_x)$, $b_{nj}(t_x)$, etc. These operations yield the following results:

(1) For $n = 1$

$$\begin{aligned}
a_{1j}(t_x) &= \beta_{1j}\sigma^{\infty}_{xx} + \beta_{2j}\sigma^{\infty}_{yy} \\
&\quad - \frac{k_1}{k_2k_3R_j}\gamma_{2j}\Big[\big\{2k_2\big(2k_3\mu_j + (k_1k_{1j} + k_2k_{2j} - k_2)\mu\big) + (\mu + k_3\mu_j)\big\}A_{1j}(u_x) \\
&\quad - \big\{2k_2\big(k_1k_{2j} + k_2k_{1j} - k_1\big)\mu - (\mu + k_3\mu_j)\big\}B_{1j}(u_y)\Big] \\
&\quad + \frac{1}{R_j}\gamma_{2j}\big[(k_{1j}\mu + 2k_1\mu_j)a_{1j}(\Delta u_x) + (2k_2\mu_j + (1 - k_{2j})\mu)b_{1j}(\Delta u_y)\big] \\
b_{1j}(t_x) &= \beta_{3j}\sigma^{\infty}_{xy} - \frac{2k_1}{R_j}\gamma_{1j}\big[A_{1j}(u_y) + B_{1j}(u_x)\big] + \frac{1}{R_j}\gamma_{1j}\big[a_{1j}(\Delta u_y) + b_{1j}(\Delta u_x)\big] \\
a_{1j}(t_y) &= \beta_{3j}\sigma^{\infty}_{xy} - \frac{2k_1}{R_j}\gamma_{1j}\big[A_{1j}(u_y) + B_{1j}(u_x)\big] + \frac{1}{R_j}\gamma_{1j}\big[a_{1j}(\Delta u_y) + b_{1j}(\Delta u_x)\big] \\
b_{1j}(t_y) &= \beta_{2j}\sigma^{\infty}_{xx} + \beta_{1j}\sigma^{\infty}_{yy} \\
&\quad + \frac{k_1}{k_2k_3R_j}\gamma_{2j}\Big[\big\{2k_2\big(k_1k_{2j} + k_2k_{1j} - k_1\big)\mu - (\mu + k_3\mu_j)\big\}A_{1j}(u_x) \\
&\quad - \big\{2k_2\big(2k_3\mu_j + (k_1k_{1j} + k_2k_{2j} - k_2)\mu\big) + (\mu + k_3\mu_j)\big\}B_{1j}(u_y)\Big] \\
&\quad + \frac{1}{R_j}\gamma_{2j}\big[(2k_2\mu_j + (1 - k_{2j})\mu)a_{1j}(\Delta u_x) + (k_{1j}\mu + 2k_1\mu_j)b_{1j}(\Delta u_y)\big]
\end{aligned} \tag{27}$$

(2) For $n > 1$

$$
\begin{aligned}
a_{nj}(t_x) &= -\frac{2k_1 n}{k_3 R_j}\gamma_{3j}\left[(k_3\mu_j + (k_1k_{1j} + k_2k_{2j})\mu)A_{nj}(u_x) - (k_1k_{2j} + k_2k_{1j})\mu B_{nj}(u_y)\right] \\
&\quad + \frac{n}{R_j}\gamma_{3j}\left[(k_1\mu_j + k_{1j}\mu)a_{nj}(\Delta u_x) + (k_2\mu_j - k_{2j}\mu)b_{nj}(\Delta u_y)\right] \\
b_{nj}(t_x) &= -\frac{2k_1 n}{k_3 R_j}\gamma_{3j}\left[(k_1k_{2j} + k_2k_{1j})\mu A_{nj}(u_y) + (k_3\mu_j + (k_1k_{1j} + k_2k_{2j})\mu)B_{nj}(u_x)\right] \\
&\quad + \frac{n}{R_j}\gamma_{3j}\left[-(k_2\mu_j - k_{2j}\mu)a_{nj}(\Delta u_y) + (k_1\mu_j + k_{1j}\mu)b_{nj}(\Delta u_x)\right] \\
a_{nj}(t_y) &= -\frac{2k_1 n}{k_3 R_j}\gamma_{3j}\left[(k_3\mu_j + (k_1k_{1j} + k_2k_{2j})\mu)A_{nj}(u_y) + (k_1k_{2j} + k_2k_{1j})\mu B_{nj}(u_x)\right] \\
&\quad + \frac{n}{R_j}\gamma_{3j}\left[(k_1\mu_j + k_{1j}\mu)a_{nj}(\Delta u_y) - (k_2\mu_j - k_{2j}\mu)b_{nj}(\Delta u_x)\right] \\
b_{nj}(t_y) &= -\frac{2k_1 n}{k_3 R_j}\gamma_{3j}\left[-(k_1k_{2j} + k_2k_{1j})\mu A_{nj}(u_x) + (k_3\mu_j + (k_1k_{1j} + k_2k_{2j})\mu)B_{nj}(u_y)\right] \\
&\quad + \frac{n}{R_j}\gamma_{3j}\left[(k_2\mu_j - k_{2j}\mu)a_{nj}(\Delta u_x) + (k_1\mu_j + k_{1j}\mu)b_{nj}(\Delta u_y)\right]
\end{aligned}
\tag{28}
$$

where

$$
\begin{aligned}
\beta_{1j} &= \frac{2k_{2j}\mu^2 + \left(k_1 - 2k_2(1-k_{2j})\right)\mu\mu_j - (1+k_2k_3)\mu_j^2}{2(\mu + k_3\mu_j)(k_{2j}\mu + \mu_j)} \\
\beta_{2j} &= \frac{k_1\mu_j((1-2k_2)\mu_j - (1-2k_{2j})\mu)}{2(\mu + k_3\mu_j)(k_{2j}\mu + \mu_j)} \\
\beta_{3j} &= \frac{\mu - \mu_j}{\mu + k_3\mu_j}
\end{aligned}
\tag{29}
$$

and

$$
\begin{aligned}
\gamma_{1j} &= \frac{\mu\mu_j}{\mu + k_3\mu_j} \\
\gamma_{2j} &= \frac{1}{k_{2j}\mu + \mu_j}\gamma_{1j} \\
\gamma_{3j} &= \frac{2}{k_{3j}\mu + \mu_j}\gamma_{1j}
\end{aligned}
\tag{30}
$$

in which

$$
k_{3j} = k_{1j} + k_{2j} = 3 - 4\nu_j \tag{31}
$$

Apart from minor notational differences and the presence of the terms involving Fourier coefficients for the displacement discontinuities, Eqs. (27) and (28) are the same as the results given previously (Crouch and Mogilevskaya, 2003). We remark that these expressions are valid for the limiting case in which $\mu_j = 0$, i.e. the jth "inclusion" is an empty hole with a traction-free boundary. In this case, of course, the formulas in Appendix B are not applicable and concept of a displacement discontinuity is not meaningful. The quantities $a_{nj}(\Delta u_x)$, $b_{nj}(\Delta u_x)$, etc. should accordingly be set equal to zero if $\mu_j = 0$.

4. The algorithm

We adopt an iterative solution algorithm to find the unknown Fourier coefficients for a general problem involving multiple inclusions. As in the approach described by Crouch and Mogilevskaya (2003), the basic algorithm relies on the repeated use of (18) and (19) to update the values of the Fourier coefficients for the displacements on the walls of the holes, given trial values of the traction coefficients. Unlike the approach described previously, however, we now also include trial values of the Fourier coefficients for displacement discontinuities in the computations. The manner in which these coefficients are updated is a key feature of the new algorithm.

4.1. Mohr–Coulomb condition

We assume that interface slip and separation can be represented by a "cohesive crack" model (Bažant and Planas, 1998), patterned after the original work of Dugdale (1960) and Barenblatt (1962). We further assume that the slip and separation processes are governed by the classical Mohr–Coulomb yield condition with a tensile strength cut-off:

$$|\sigma_{r\theta}| \leqslant c - \sigma_{rr} \tan\phi; \quad \sigma_{rr} \leqslant T \tag{32}$$

where c, ϕ, and T are respectively the cohesion, angle of friction, and tensile strength of an inclusion/matrix interface, with $0 \leqslant T \leqslant c\cot\phi$, as depicted in Fig. 2. For normal stresses σ_{rr} less than the tensile strength, the interface shear stress $\sigma_{r\theta}$ cannot exceed the value specified in (32). To meet this constraint, the interface must be allowed to undergo a certain amount of localized inelastic deformation, or permanent slip, in the transverse direction. The normal stress σ_{rr} cannot exceed the tensile strength T, and, to meet this constraint, the interface must be allowed to crack apart. Both circumstances require the introduction of displacement discontinuities along the affected portions of the interface.

Implementation of the Mohr–Coulomb constraint (32) requires an incremental approach. In order to simplify the presentation of the method, however, we will explain the procedure for a single loading increment. The same methodology can be applied to successive loading (or unloading) increments.

4.2. Computation of the Fourier coefficients

To begin the solution procedure a value must be chosen for the number of terms N_k in the Fourier series for the displacements, tractions, and displacement discontinuities for each inclusion, $k = 1$ to K. All of the

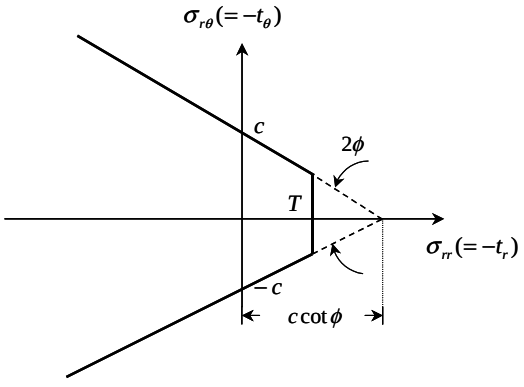

Fig. 2. Mohr–Coulomb envelope with tension cut-off.

Fourier coefficients are then initialized by setting them equal to zero for $n = 1$ to N_k. The value of N_k for any inclusion can be increased during the iteration process if it is found that additional accuracy is needed (Crouch and Mogilevskaya, 2003).

For each cycle of iteration p, the Fourier coefficients are updated as follows:

Step 1. Use (27) and (28) to compute the trial traction coefficients $a_{nj}^{(p)}(t_x)$, $b_{nj}^{(p)}(t_x)$, $a_{nj}^{(p)}(t_y)$, and $b_{nj}^{(p)}(t_y)$ at the jth inclusion due to the influences of *all the other* inclusions, $k = 1$ to K, $k \neq j$, as well as the stresses at infinity and the *current values* of the displacement discontinuity coefficients $a_{nj}^{(p-1)}(\Delta u_x)$, $b_{nj}^{(p-1)}(\Delta u_x)$, $a_{nj}^{(p-1)}(\Delta u_y)$, and $b_{nj}^{(p-1)}(\Delta u_y)$. For the first cycle of iteration, this is equivalent to treating each inclusion as a perfectly bonded, isolated entity.

Step 2. Use Eq. (3) (with k replaced by j) to compute the trial tractions $t_x^{(p)}$ and $t_y^{(p)}$ at M_j equally spaced points along the boundary of the jth inclusion (where $M_j \geqslant N_j$), and then compute the local normal and shear components of these quantities $t_r^{(p)}$ and $t_\theta^{(p)}$ at each point using the transformation equations

$$\begin{aligned} t_r^{(p)}(R_j,\theta_{mj}) &= t_x^{(p)}(R_j,\theta_{mj})\cos\theta_{mj} + t_y^{(p)}(R_j,\theta_{mj})\sin\theta_{mj} \\ t_\theta^{(p)}(R_j,\theta_{mj}) &= -t_x^{(p)}(R_j,\theta_{mj})\sin\theta_{mj} + t_y^{(p)}(R_j,\theta_{mj})\cos\theta_{mj} \end{aligned} \tag{33}$$

where m ranges from 1 to M_j and where $\theta_{mj} = 2\pi(m-1)/M_j$. It should be noted that trial tractions (33) are estimates of the total, or resultant, tractions at each point m; that is, these quantities represent the sums of the initial tractions and the traction changes due to the presence of the K inclusions. It should also be noted that positive values of the tractions t_r and t_θ on the wall of the hole correspond to negative stress tensor components σ_{rr} and $\sigma_{r\theta}$, i.e. $t_r = -\sigma_{rr}$ and $t_\theta = -\sigma_{r\theta}$.

Step 3. Use (32) and (33) to compute an adjusted set of tractions t_r^* and t_θ^* for each of the M_j discrete points to take account of localized yielding:

(a) If $-t_r^{(p)}(R_j,\theta_{mj}) \leqslant T$ and $|t_\theta^{(p)}(R_j,\theta_{mj})| \leqslant c_j + t_r^{(p)}(R_j,\theta_{mj})\tan\phi_j$ set

$$\begin{aligned} t_\theta^*(R_j,\theta_{mj}) &= t_\theta^{(p)}(R_j,\theta_{mj}) \\ t_r^*(R_j,\theta_{mj}) &= t_r^{(p)}(R_j,\theta_{mj}) \end{aligned} \tag{34}$$

(b) If $-t_r^{(p)}(R_j,\theta_{mj}) \leqslant T$ and $|t_\theta^{(p)}(R_j,\theta_{mj})| > c_j + t_r^{(p)}(R_j,\theta_{mj})\tan\phi_j$ set

$$\begin{aligned} t_\theta^*(R_j,\theta_{mj}) &= \operatorname{sign}\left(t_\theta^{(p)}(R_j,\theta_{mj})\right)\left(c_j + t_r^{(p)}(R_j,\theta_{mj})\tan\phi_j\right) \\ t_r^*(R_j,\theta_{mj}) &= t_r^{(p)}(R_j,\theta_{mj}) \end{aligned} \tag{35}$$

(c) If $-t_r^{(p)}(R_j,\theta_{mj}) > T$ set

$$\begin{aligned} t_\theta^*(R_j,\theta_{mj}) &= 0 \\ t_r^*(R_j,\theta_{mj}) &= 0 \end{aligned} \tag{36}$$

Condition (a) means that the trial tractions for point m lie within the Mohr–Coulomb envelope and therefore do not require any adjustment; (b) means that the indicated combination of trial tractions lies outside the envelope and hence the value of the transverse (shear) component is set equal to the yield stress associated with the prevailing normal traction. Finally, condition (c) represents tensile failure at point m, in which case the tractions at this point of the interface are set equal to zero.

Step 4. Compute the x and y components of the adjusted traction *changes* using the inverse of transformation (33) and eliminating the initial tractions due to the stresses at infinity:

$$t_x^*(R_j,\theta_{mj}) = t_r^*(R_j,\theta_{mj})\cos\theta_{mj} - t_\theta^*(R_j,\theta_{mj})\sin\theta_{mj} + (\sigma_{xx}^\infty\cos\theta_{mj} + \sigma_{xy}^\infty\sin\theta_{mj})$$
$$t_y^*(R_j,\theta_{mj}) = t_r^*(R_j,\theta_{mj})\sin\theta_{mj} + t_\theta^*(R_j,\theta_{mj})\cos\theta_{mj} + (\sigma_{xy}^\infty\cos\theta_{mj} + \sigma_{yy}^\infty\sin\theta_{mj}) \tag{37}$$

in which $m = 1$ to M_j.

Step 5. Compute the Fourier coefficients associated with t_x^* and t_y^* using the formulas

$$a_{nj}^*(t_x) = \frac{2}{M_j}\sum_{m=1}^{M_j} t_x^*(R_j,\theta_{mj})\cos n\theta_{mj};\quad b_{nj}^*(t_x) = \frac{2}{M_j}\sum_{m=1}^{M_j} t_x^*(R_j,\theta_{mj})\sin n\theta_{mj}$$
$$a_{nj}^*(t_y) = \frac{2}{M_j}\sum_{m=1}^{M_j} t_y^*(R_j,\theta_{mj})\cos n\theta_{mj};\quad b_{nj}^*(t_y) = \frac{2}{M_j}\sum_{m=1}^{M_j} t_y^*(R_j,\theta_{mj})\sin n\theta_{mj} \tag{38}$$

These equations are derived in Appendix C using a least squares approach patterned after the work of Barnes and Janković (1999). Eq. (38) are discrete forms of the usual integral definitions of the Fourier coefficients (cf. (17)). Barnes and Janković recommend using the value $M_j = 4N_j$, and we have followed this advice in all of the examples discussed below.

Step 6. Substitute (38) into (18) and (19) to update the Fourier coefficients for the displacements of the boundary of the jth hole for the pth iteration, i.e. compute $a_{nj}^{(p)}(u_x)$, $b_{nj}^{(p)}(u_x)$, $a_{nj}^{(p)}(u_y)$, and $b_{nj}^{(p)}(u_y)$ for $n = 1$ to N_j.

Step 7. Similarly, substitute (38) into (22), (24), and (25)to update the Fourier coefficients for the displacements of the boundary of the jth *disc*, i.e. compute $a_{nj}^{\prime(p)}(u_x)$, $b_{nj}^{\prime(p)}(u_x)$, $a_{nj}^{\prime(p)}(u_y)$, and $b_{nj}^{\prime(p)}(u_y)$ for $n = 1$ to N_j.

Step 8. Use Eqs. (13)–(16) (with k replaced by j) to compute trial displacement discontinuities $\Delta u_x^{(p)}$ and $\Delta u_y^{(p)}$ at M_j equally spaced points along the boundary of the jth inclusion (where again $M_j \geqslant N_j$), and then compute the local normal and shear components of these quantities $\Delta u_r^{(p)}$ and $\Delta u_\theta^{(p)}$ at each point using transformation equations analogous to (33).

Step 9. Compute an adjusted set of displacement discontinuities Δu_r^* and Δu_θ^* at each of the M_j discrete points to prohibit overlapping and/or allow for the occurrence of localized cracking or slip:

(a) If cracking has occurred at the point (R_j,θ_{mj}) and if $\Delta u_r^{(p)}(R_j,\theta_{mj}) < 0$ then, to prohibit overlapping, set

$$\Delta u_r^*(R_j,\theta_{mj}) = 0$$
$$\Delta u_\theta^*(R_j,\theta_{mj}) = \Delta u_\theta^{(p)}(R_j,\theta_{mj}) \tag{39}$$

(b) If cracking has occurred and if $\Delta u_r^{(p)}(R_j,\theta_{mj}) \geqslant 0$ set

$$\Delta u_r^*(R_j,\theta_{mj}) = \Delta u_r^{(p)}(R_j,\theta_{mj})$$
$$\Delta u_\theta^*(R_j,\theta_{mj}) = \Delta u_\theta^{(p)}(R_j,\theta_{mj}) \tag{40}$$

(c) If cracking has not occurred and no slip has taken place, then, to maintain bonding at the point, set

$$\Delta u_r^*(R_j,\theta_{mj}) = 0$$
$$\Delta u_\theta^*(R_j,\theta_{mj}) = 0 \tag{41}$$

(d) If cracking has not occurred but slip has taken place set

$$\Delta u_r^*(R_j,\theta_{mj}) = 0$$
$$\Delta u_\theta^*(R_j,\theta_{mj}) = \Delta u_\theta^{(p)}(R_j,\theta_{mj}) \tag{42}$$

Step 10. Compute the x and y components of the adjusted displacement discontinuities at the points (R_j, θ_{mj}), $m = 1$ to M_j, and then find the Fourier coefficients associated with Δu_x^* and Δu_y^* using the formulas (cf. (38))

$$\begin{aligned} a_{nj}^*(\Delta u_x) &= \frac{2}{M_j}\sum_{m=1}^{M_j}\Delta u_x^*(R_j,\theta_{mj})\cos n\theta_{mj}; \quad b_{nj}^*(\Delta u_x) = \frac{2}{M_j}\sum_{m=1}^{M_j}\Delta u_x^*(R_j,\theta_{mj})\sin n\theta_{mj} \\ a_{nj}^*(\Delta u_y) &= \frac{2}{M_j}\sum_{m=1}^{M_j}\Delta u_y^*(R_j,\theta_{mj})\cos n\theta_{mj}; \quad b_{nj}^*(\Delta u_y) = \frac{2}{M_j}\sum_{m=1}^{M_j}\Delta u_y^*(R_j,\theta_{mj})\sin n\theta_{mj} \end{aligned} \tag{43}$$

These quantities then define the current values of the displacement discontinuity coefficients in Step 1.

Step 11. Continue this process until the largest change in the coefficients between two successive iterates is less than a small number ε, i.e. until $\left|a_{nj}^{(p)}(u_x) - a_{nj}^{(p-1)}(u_x)\right| \leqslant \varepsilon$, $\left|a_{nj}^{(p)}(u_y) - a_{nj}^{(p-1)}(u_y)\right| \leqslant \varepsilon$, etc. for all n and for every inclusion. In most problems examined to date we have taken ε as 10^{-4} times the magnitude of the largest Fourier coefficient associated with the initial displacements (obtained from the first groups of terms in (1)).

4.3. Successive over-relaxation

The iteration process can be made to converge faster—or in some cases made to converge when it would otherwise not—by using the method of successive over-relaxation (Golub and Van Loan, 1996; Varga, 2000). This is accomplished by modifying the calculations in Steps 6 and 7 above, as follows.

First, let $a_{nj}^*(u_x)$, $b_{nj}^*(u_x)$, etc. be the trial Fourier coefficients for the displacements of the boundary of the jth hole associated with the trial traction coefficients $a_{nj}^*(t_x)$, $b_{nj}^*(t_x)$, etc. from (38). (In Step 6 of the unmodified procedure the trial coefficients for the displacements are simply called $a_{nj}^{(p)}(u_x)$, $b_{nj}^{(p)}(u_x)$, etc.) Similarly, let $a_{nj}'^*(u_x)$, $b_{nj}'^*(t_x)$ be the trial Fourier coefficients for the displacements of the boundary of the jth disc associated with the same trial traction coefficients. Then, use the following relations to compute the updated displacement coefficients for the pth iteration:

$$a_{nj}^{(p)}(u_x) = a_{nj}^{(p-1)}(u_x) + \omega\left[a_{nj}^*(u_x) - a_{nj}^{(p-1)}(u_x)\right] \quad \text{etc.} \tag{44}$$

$$a_{nj}'^{(p)}(u_x) = a_{nj}'^{(p-1)}(u_x) + \omega\left[a_{nj}'^*(u_x) - a_{nj}'^{(p-1)}(u_x)\right] \quad \text{etc.} \tag{45}$$

In these equations ω is the over-relaxation factor, which lies in the range $0 < \omega < 2$ (Varga, 2000). When $\omega = 1$ the results calculated from (44) and (45) are the same as those that would be calculated in Steps 6 and 7 of the original procedure. When ω is less than 1 it is referred to as an *under-relaxation* factor. Under-relaxation is often needed to achieve convergence for non-linear problems, and we have found that this is generally the case for our algorithm, too.

5. Examples

5.1. Crack along the interface of a single inclusion

Toya (1974) derived the analytical solution for the problem of a traction-free, arc-shaped crack along the interface of a circular elastic inclusion in an infinite plane. The solution is valid for a restricted range of

crack lengths and combinations of applied stresses at infinity for which the crack faces do not come into contact (these conditions are carefully delineated in Toya's paper). The solution could actually be considered as approximate in the sense that the displacement discontinuities exhibit oscillations very close to the crack tips, which entails a physically impossible localized overlapping of the crack faces (see, for example, Chao and Laws, 1997), but consideration of this aspect of the problem is beyond the scope of the present discussion.

While our Fourier series solution does not attempt to represent crack tip asymptotics, it is instructive to see the extent to which it can approximate Toya's results. It is also useful to note that our numerical approach can easily accommodate situations for which the crack faces come into contact. Illustrations of these matters are given below.

Following Toya (1974), we consider a crack subtending an angle 2α along the interface of a glass inclusion ($\nu' = 0.22$, $\mu' = 44.2$ GN/m^2) of radius a in an epoxy matrix ($\nu = 0.35$, $\mu = 2.39$ GN/m^2), with a uniaxial tensile stress σ_0 applied at an angle φ from the x-axis, as shown in Fig. 3. Guided by Toya's results, we take both α and φ as 30° to ensure that the crack is open along its entire length (not including the small regions close to the crack tips). In addition, we take $\phi = 0$, $c \gg \sigma_0$, and $T \gg \sigma_0$ to ensure that the inclusion is perfectly bonded over the uncracked part of its interface. The uniaxial tension σ_0 at infinity is achieved by taking $\sigma^{\infty}_{xx} = 0.75\sigma_0$, $\sigma^{\infty}_{yy} = 0.25\sigma_0$, and $\sigma^{\infty}_{xy} = 0.433\sigma_0$.

The numerical procedure described in Section 4 was modified to require that the crack faces be traction free, and the problem was solved by taking $N = 45$ and using the iteration parameters $\varepsilon = 10^{-4}$ and $\omega = 0.5$ (i.e. under-relaxation). With these parameters, the numerical solution took 16 iterations. The computed distributions of the radial and shear stresses σ_{rr}/σ_0 and $\sigma_{r\theta}/\sigma_0$ on the interface are compared with Toya's analytical solution in Fig. 4; the corresponding results for the displacement discontinuities $\Delta u_r/a$ and $\Delta u_\theta/a$ for the particular case $\sigma_0 = 1.0$ MN/m^2 are shown in Fig. 5.

It is apparent from Figs. 4 and 5 that the numerical solution for this problem is rather crude. The computed stresses (Fig. 4) clearly exhibit the Gibbs phenomenon as a result of the abrupt changes in σ_{rr} and $\sigma_{r\theta}$ that occur between the cracked and uncracked portions of the interface. The displacement discontinuities (Fig. 5) are also affected, but to a lesser extent. Moreover, the computed values of σ_{rr} and $\sigma_{r\theta}$ along the cracked portions of the interface are evidently only zero in an average sense.

The Gibbs phenomenon is inherent in Fourier series representations of functions with jump discontinuities (Jerri, 1998). Although the phenomenon cannot be eliminated entirely, several methods have been developed for filtering it out, including a simple but effective approach due to Lanczos (1966). Lanczos's

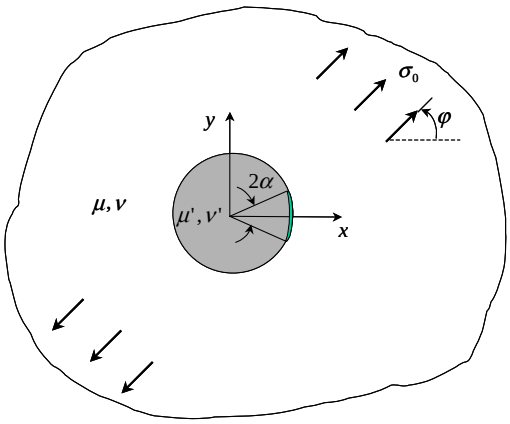

Fig. 3. Geometry for inclusion with interface crack.

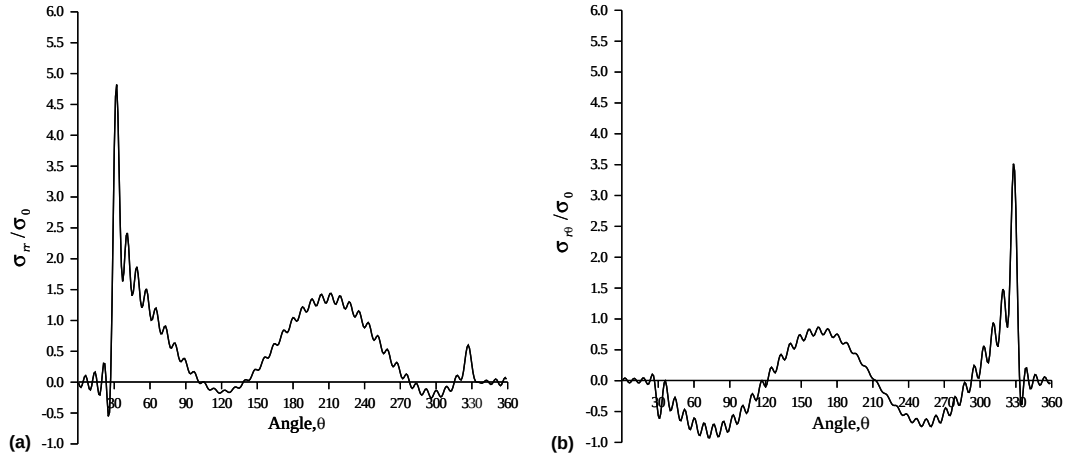

Fig. 4. Computed radial (a) and shear (b) stresses exhibiting Gibbs phenomenon; $N = 45$.

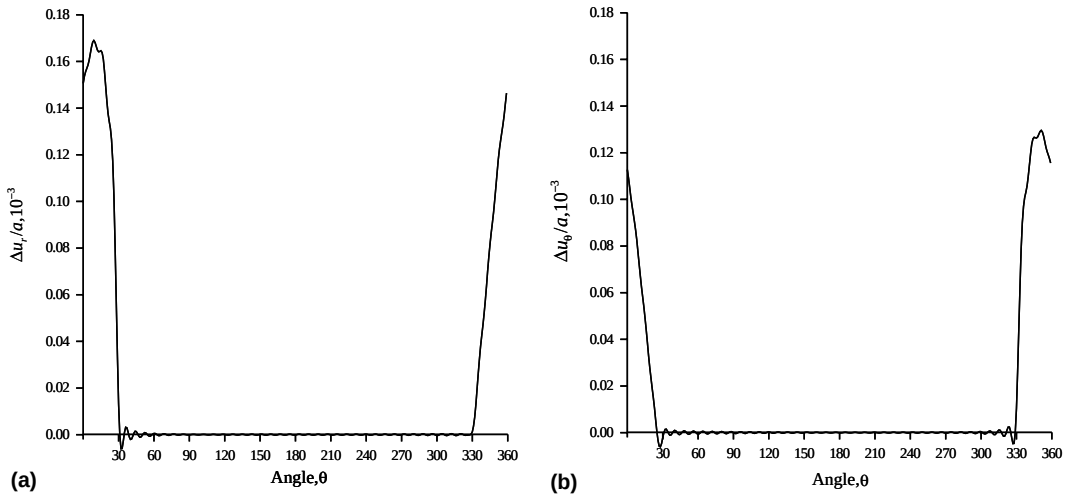

Fig. 5. Computed radial (a) and shear (b) components of displacement discontinuity exhibiting Gibbs phenomenon; $N = 45$.

"method of local smoothing" for a truncated Fourier series is derived by analytically integrating the series term by term and then differentiating it numerically using a central differencing scheme with a step size chosen so as to minimize the oscillations in the vicinity of a jump discontinuity. If the Nth partial sum of a Fourier series representation of a function $f(\theta)$ with a jump discontinuity is $f_N(\theta)$, i.e. if

$$f_N(\theta) = a_0 + \sum_{n=1}^{N} (a_n \cos n\theta + b_n \sin n\theta) \tag{46}$$

the locally smoothed value of $f_N(\theta)$ is given as follows (Lanczos, 1966):

$$\overline{f}_N(\theta) = a_0 + \sum_{n=1}^{N} \frac{\sin(n\pi/N)}{n\pi/N} (a_n \cos n\theta + b_n \sin n\theta) \tag{47}$$

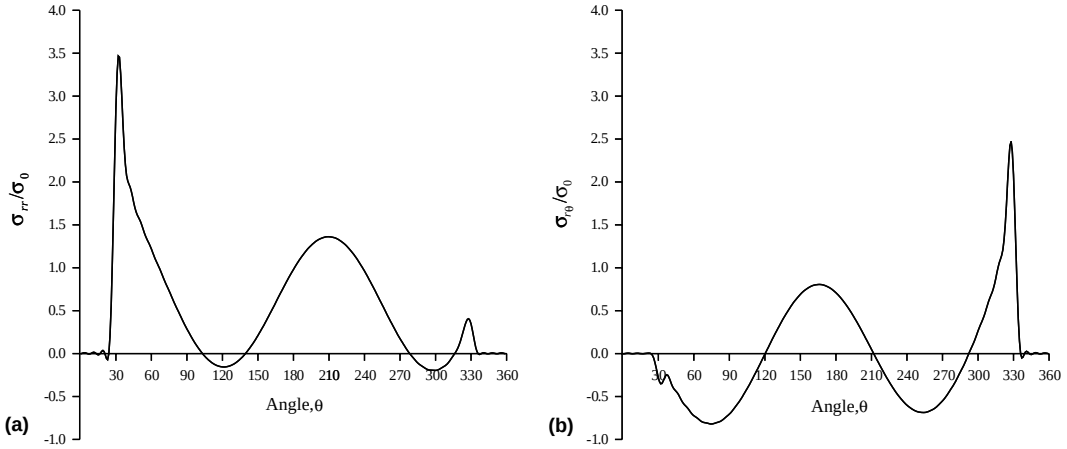

Fig. 6. Locally smoothed values of radial (a) and shear (b) stresses from Fig. 4(a) and (b).

Applying this algorithm to the Fourier series approximations for the stresses σ_{rr}/σ_0 and $\sigma_{r\theta}/\sigma_0$ in Fig. 4, we obtain the results shown in Fig. 6. The Lanczos local smoothing technique effectively eliminates the fluctuations in the stresses noticed previously. Further improvement can be achieved by incorporating the smoothing algorithm within the iterative procedure to ensure that the most accurate possible estimates of the trial tractions and displacement discontinuities are computed in Steps 2 and 8 of the procedure. Repeating the preceding calculations with these changes, we obtain the results shown in Figs. 7 and 8. Figs. 9–12 give comparable results for $N = 90$ and $N = 180$. The three sets of calculations were performed using $\varepsilon = 10^{-4}$ and $\omega = 0.5$ and required 16, 17, and 17 iterations for $N = 45$, 90, and 180, respectively.

In solving this problem, no attempt was made to optimize the number of terms in the Fourier series representations for the tractions, displacements, and displacement discontinuities. It is useful to note, however, that a solution obtained with $N = 90$ is essentially the same as that obtained with $N = 180$, whereas a solution with $N = 45$, although generally reasonable, is significantly less accurate.

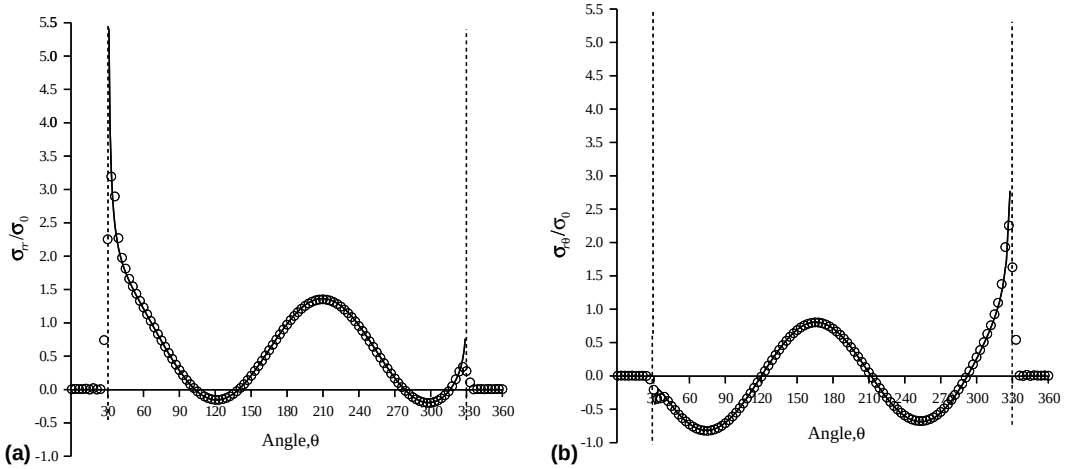

Fig. 7. Computed radial (a) and shear (b) stresses (open circles) compared with analytical solution (solid lines) for $N = 45$.

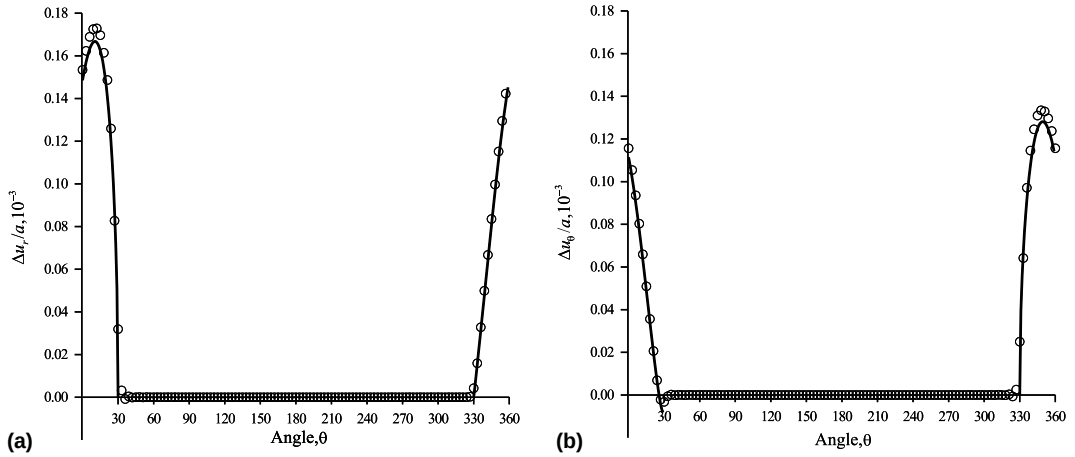

Fig. 8. Computed radial (a) and shear (b) components of displacement discontinuity (open circles) compared with analytical solution (solid lines) for $N = 45$.

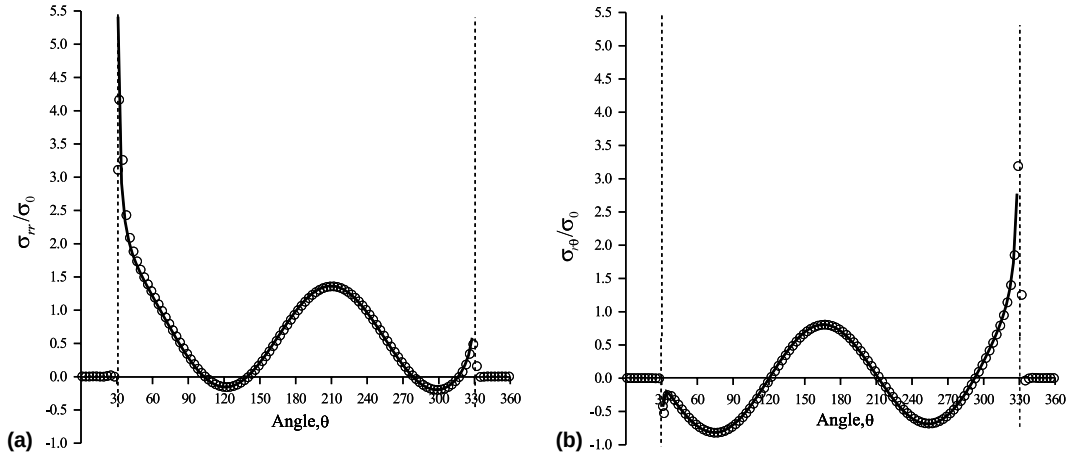

Fig. 9. Computed radial (a) and shear (b) stresses (open circles) compared with analytical solution (solid lines) for $N = 90$.

If angle α is greater than approximately 35° and all other physical and geometric aspects of the problem are unchanged, the crack faces will come into contact in the vicinity of one crack tip (the one at angle $\theta = 360° - \alpha$). This is the limit of validity of Toya's solution. In order to demonstrate the utility of our numerical approach, we consider a much larger value of this angle, $\alpha = 90°$, and repeat the calculations, assuming zero friction in the zone of contact. The results for the stresses and displacement discontinuities are given in Fig. 13. It can be seen from Fig. 13(b) that the crack is closed for θ between approximately 270° and 310° but is otherwise open. Fig. 13(a) shows that the radial stress is compressive ($\sigma_{rr} < 0$) in the zone of contact, as expected.

We conclude from this example that our numerical procedure accurately predicts the tractions and displacement discontinuities for an inclusion with an interface crack, provided a sufficiently large number of terms is taken in the Fourier series representations of these quantities.

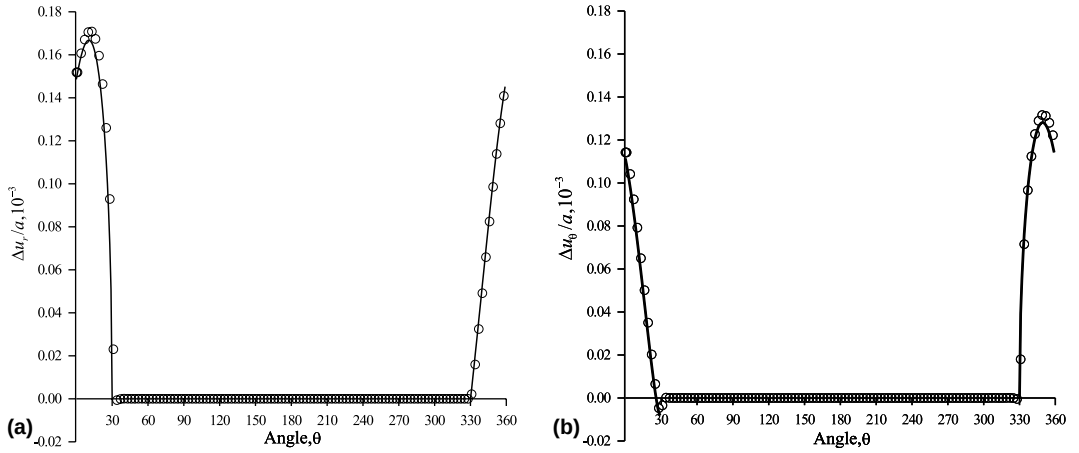

Fig. 10. Computed radial (a) and shear (b) components of displacement discontinuity (open circles) compared with analytical solution (solid lines) for $N = 90$.

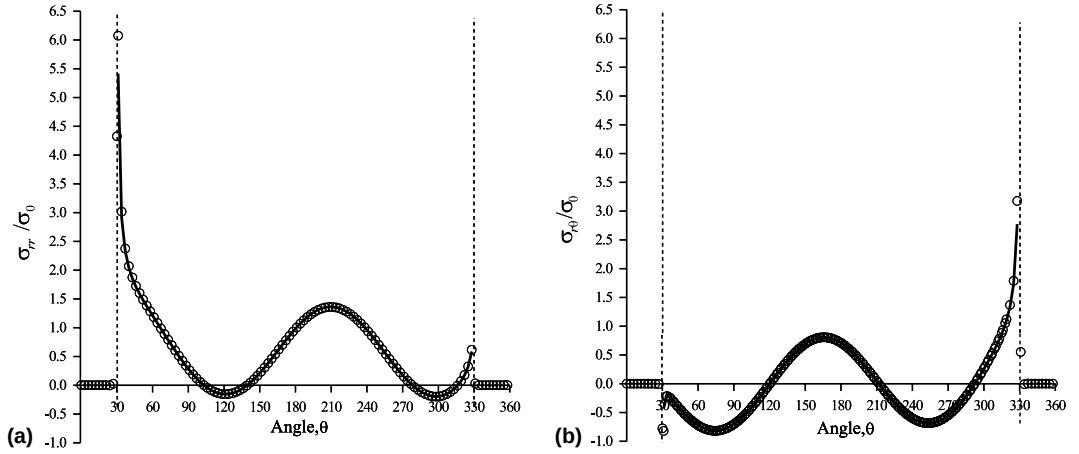

Fig. 11. Computed radial (a) and shear (b) stresses (open circles) compared with analytical solution (solid lines) for $N = 180$.

5.2. Debonding of a smooth inclusion

The analytical solution is available for an unbonded, smooth (i.e. frictionless) circular inclusion with elastic constants $\nu' = \nu$ and $\mu' = \mu$ in an elastic plate under uniaxial tension $\sigma_{yy}^{\infty} = \sigma_0$ at infinity (Stippes et al., 1962). Under the prevailing stress state the inclusion separates from the plate over a portion of its periphery, but is in contact over the arcs $-\eta \leqslant \theta \leqslant \eta$ and $\pi + \eta \leqslant \theta \leqslant \pi - \eta$. The contact angle η is independent of the elastic constants ν and μ (Stippes et al., 1962). Because of symmetry we will restrict our attention to one-quarter of the circle, $0 \leqslant \theta \leqslant \pi/2$. (We note that Sheremet'ev (1952) considered the more general case of an unbonded, smooth inclusion with elastic constants $\nu' \neq \nu$ and $\mu' \neq \mu$ but did not present any numerical results. Later, Noble and Hussain (1969) treated the same problem, also without giving any numerical results.)

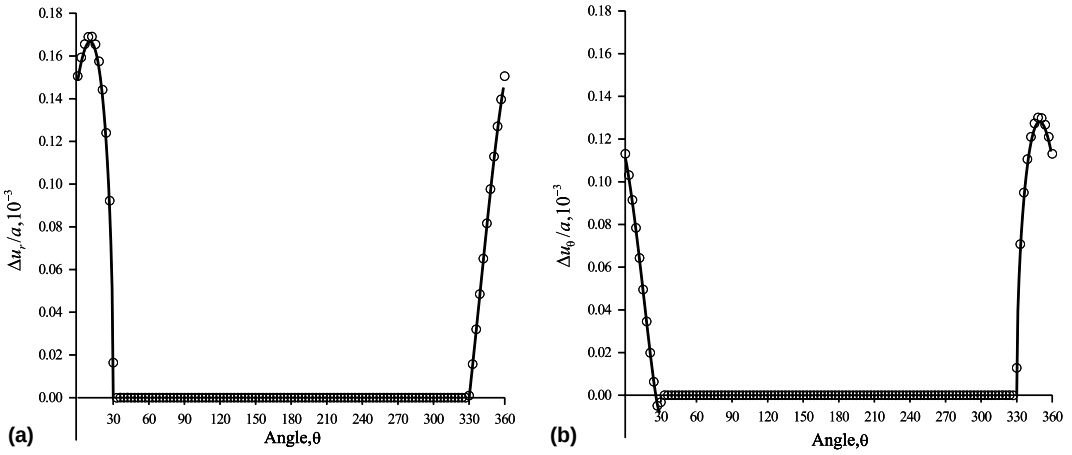

Fig. 12. Computed radial (a) and shear (b) components of displacement discontinuity (open circles) compared with analytical solution (solid lines) for $N = 180$.

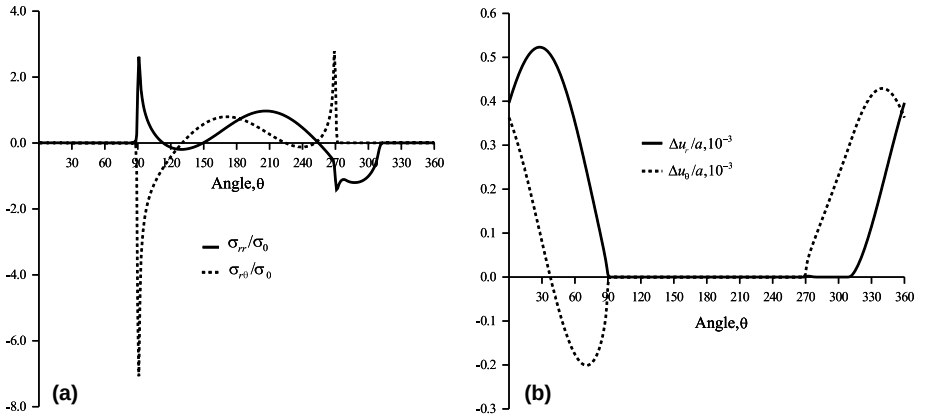

Fig. 13. Stresses (a) and displacement discontinuities (b) for partially closed crack.

The subject problem can be solved numerically using the iterative procedure described in Section 4. A frictionless, no-tension interface is modeled by taking the Mohr–Coulomb parameters as $c = \phi = T = 0$; the contact zones are then automatically determined by the enforcement of a no-overlap constraint during the iteration process.

The computed radial stress σ_{rr}/σ_0 in the zone of contact is compared with Stippes et al.'s solution in Fig. 14; a similar comparison for the circumferential stress $\sigma_{\theta\theta}/\sigma_0$ over one quadrant of the boundary of the *hole* is given in Fig. 15. The numerical results in these figures were obtained using $N = 180$, $\varepsilon = 10^{-4}$, and $\omega = 0.5$. The Lanczos local smoothing technique was used to filter out unwanted oscillations caused by the Gibbs phenomenon, and the solution required 18 iterations. It can be seen that the numerical results are in good agreement with the analytical solution for this problem, except that our Fourier series approach slightly overestimates the extent of the zone of contact, as can be seen in Fig. 14.

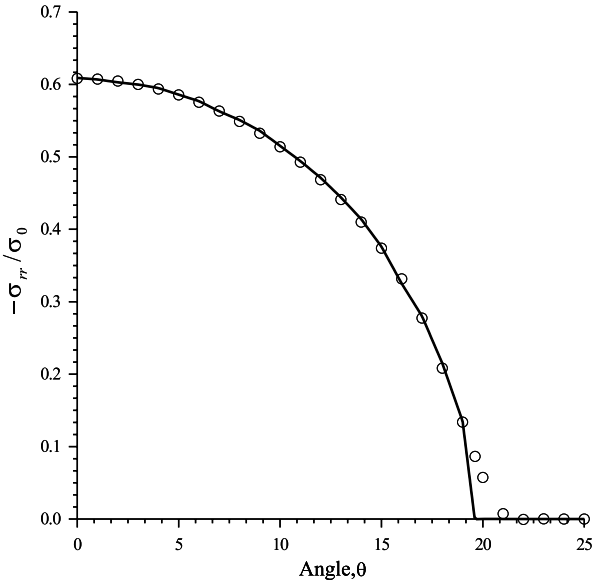

Fig. 14. Radial stress in zone of contact for smooth inclusion: solid line is analytical solution [20]; open circles are computed results.

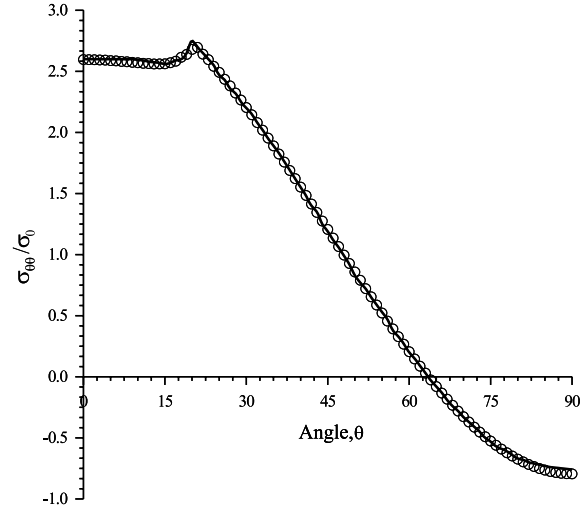

Fig. 15. Circumferential stress for smooth inclusion: solid line is analytical solution [20]; open circles are computed results.

5.3. Debonding and slip of a rough inclusion

A more serious test of our numerical algorithm concerns the situation for which the interface between the inclusion and the wall of the hole is rough. In this case, the inclusion is not free sliding and the solution of the problem depends on the coefficient of friction between the inclusion and the plate. Hussain and Pu (1971) used a variational approach to obtain a semi-analytical solution of this problem for $\nu' = \nu$ and $\mu' = \mu$, and we now compare our numerical results with theirs for the case that the coefficient of friction

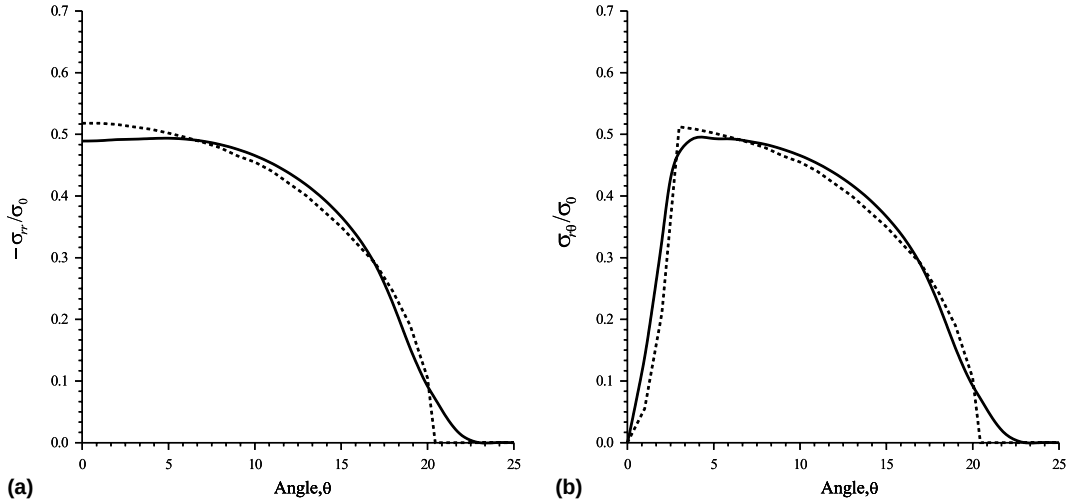

Fig. 16. Comparison of computed radial (a) and shear (b) stresses for rough inclusion: dashed lines are results from [21]; solid lines are results from Fourier series approach.

is equal to 1.0, i.e. $\phi = 45°$. As in the preceding example, the plate is loaded in uniaxial tension $\sigma_{yy}^{\infty} = \sigma_0$ at infinity.

Hussain and Pu's numerical solution for the radial stress σ_{rr}/σ_0 is reproduced in Fig. 16(a), together with our Fourier series solution (locally smoothed and obtained in 34 iterations using $N = 180$, $\varepsilon = 10^{-4}$, and $\omega = 0.5$); similar comparisons for the shear stress $\sigma_{r\theta}/\sigma_0$ are given in Fig. 16(b). It can be seen that the results are similar, although some differences do occur. For example, Hussain and Pu obtain a value of 0.52 (approximately) for the radial compression $-\sigma_{rr}/\sigma_0$ at $\theta = 0$, whereas we find the value 0.49. Also, according to Hussain and Pu, the onset of frictional sliding (where $-\sigma_{rr} = \sigma_{r\theta}$) is at $\theta = 2.49°$. By extrapolating the curve for $\sigma_{r\theta}/\sigma_0$ in Fig. 16(b) to estimate a sharp break point, we find a value of approximately 3° for our approach. In addition, as in the case of a smooth inclusion, our Fourier series approach predicts a slightly larger zone of contact. Overall, however, the results agree reasonably well, leading us to conclude that our algorithm is capable of modeling both slip and separation of the interface of a circular inclusion.

5.4. Multiple inclusions

Finally, to illustrate the capability of modeling interactions among multiple inclusions, we consider the case of four inclusions in a plane loaded by a uniaxial tensile stress $\sigma_{yy}^{\infty} = \sigma_0$ at infinity. The inclusions all have radius a and are centered on the corners of an imaginary square of side $2d$ ($d \geqslant a$), as shown in Fig. 17. As in the example in Section 5.1 we let the elastic constants of the inclusions and the matrix be $\nu' = 0.22$, $\mu' = 44.2$ GN/m^2, and $\nu = 0.35$, $\mu = 2.39$ GN/m^2, respectively. We also assume that the interfaces of the four inclusions have the same Mohr–Coulomb parameters: $c = 2\sigma_0$, $\phi = 0$, and $T = 2\sigma_0$. (We take ϕ equal to zero for modeling convenience—with this choice for the parameter it is easy to identify at a glance the portions of the interface that undergo slip.) Under these conditions, the problem is symmetric and the discussion can be limited to any one of the four inclusions, say the one centered at the point $(x, y) = (d, d)$ and labeled 1 in Fig. 17. All subsequent references to this inclusion should be understood also to apply to the other three inclusions, with appropriate allowances made for symmetry. The results presented below were obtained by taking $N = 180$ for each inclusion, with $\varepsilon = 10^{-4}$ and $\omega = 0.5$. The Lanczos local smoothing technique was again used to filter out unwanted oscillations caused by the Gibbs phenomenon.

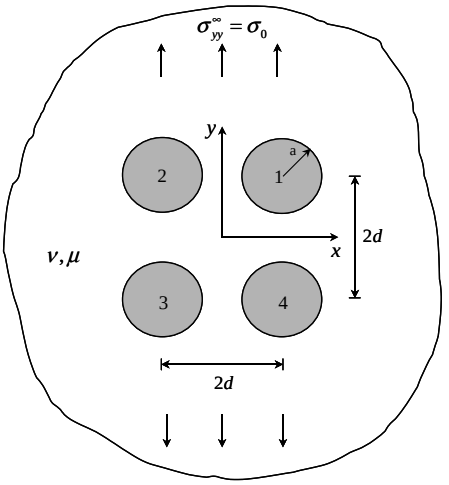

Fig. 17. Four equal sized inclusions with elastic constants ν', μ' in a plane under uniaxial tension at infinity.

We first suppose that the inclusions are far enough apart so as to be effectively isolated from one another, i.e. $d \gg a$. It can be shown that the radial and shear stresses along the interface for this case are $\sigma_{rr} = \sigma_0(0.6093–0.7859\cos 2\theta)$ and $\sigma_{r\theta} = 0.7859\sigma_0 \sin 2\theta$. The maximum radial tension is therefore $\sigma_{rr} = 1.3952\sigma_0$ (at $\theta = 90°$ and $\theta = 270°$) and the maximum shear stress is $|\sigma_{r\theta}| = 0.7859\sigma_0$ (at $\theta = \pm 45°$, $\pm 135°$). Consequently, neither debonding nor slip of the inclusion interface will occur under the assumed conditions.

Interaction effects among the inclusions become progressively more important as $d/a \to 1$. For example, if $d/a = 1.5$ the radial stress is significantly altered in the vicinity of the points where the inclusions are closest together ($\theta = 180°$ and $\theta = 270°$ for the inclusion we are considering—the one in the first quadrant). This is shown in Fig. 18, which compares the distributions of the radial and shear stresses for $d/a = 1.5$ with

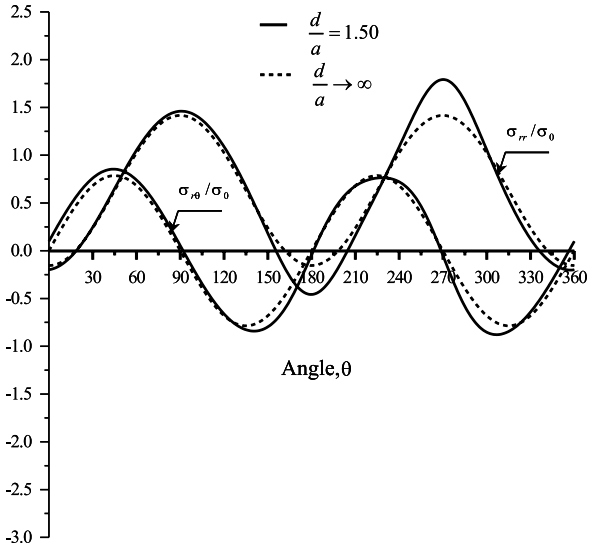

Fig. 18. Radial and shear stresses for inclusion 1 in Fig. 17 for $d/a = 1.50$ and $d/a \to \infty$.

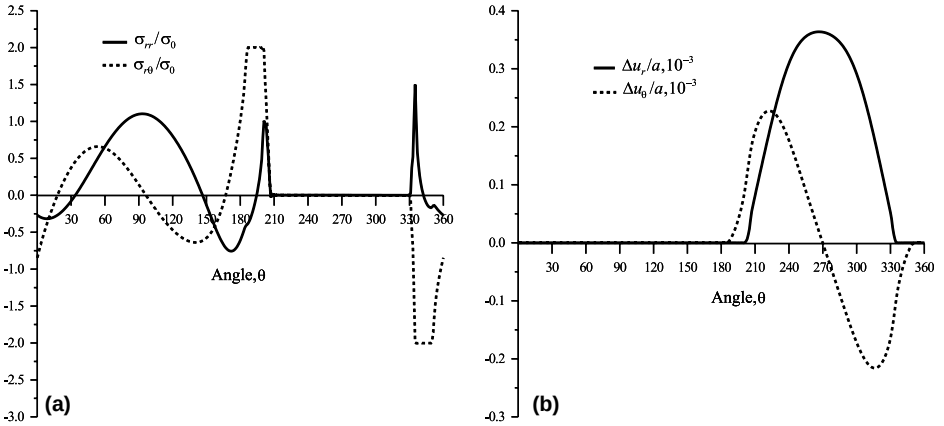

Fig. 19. Stresses (a) and displacement discontinuities (b) for inclusion 1 in Fig. 17 for $d/a = 1.315$.

the corresponding distributions of these quantities for an isolated inclusion. It can be seen that the radial stress is more affected by the presence of the other inclusions in this case than is the shear stress. Debonding and slip of the interface still do not occur.

By trial, it is found that the tensile strength of the inclusion/matrix interface is reached when $d/a = 1.315$; this occurs at the point $\theta = 270.5°$ for inclusion 1. The introduction of a small crack at this location then creates a stress-raiser that causes the crack to extend until the radial stress at each tip is less than the tensile strength $T = 2\sigma_0$. The resulting stress and displacement discontinuity distributions are given in Fig. 19(a) and (b). (The values of the displacement discontinuities correspond to the particular case for which $\sigma_0 = 1.0\ \mathrm{MN/m^2}$.) These figures show that the nature of the interfacial damage is rather complicated, even for this relatively simple problem. The portions of the interface where polar angle θ is in the range $202° \leqslant \theta \leqslant 336°$ (approximately) become debonded, because $\sigma_{rr} = 0$ and $\Delta u_r \neq 0$ over these arcs. Slip occurs over arcs of approximately 14° on either side of the zones of separation; these portions of the interface can be identified by the conditions $\sigma_{r\theta} = 2\sigma_0$ $(=c)$, $\Delta u_\theta \neq 0$, and $\Delta u_r = 0$ and $\sigma_{rr} \neq 0$. Finally, we can see that the rest of the interface remains perfectly bonded, because $\Delta u_r = \Delta u_\theta = 0$. For this simple hypothetical

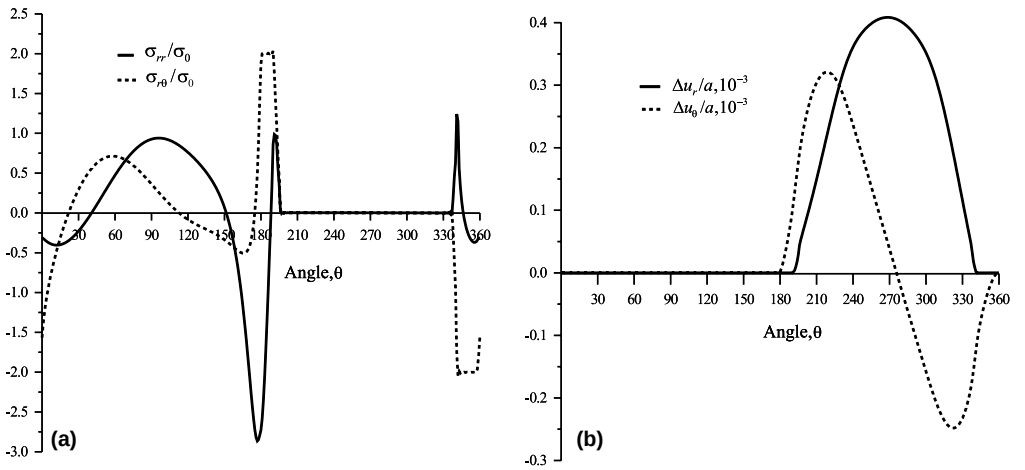

Fig. 20. Stresses (a) and displacement discontinuities (b) for inclusion 1 in Fig. 17 for $d/a = 1.05$.

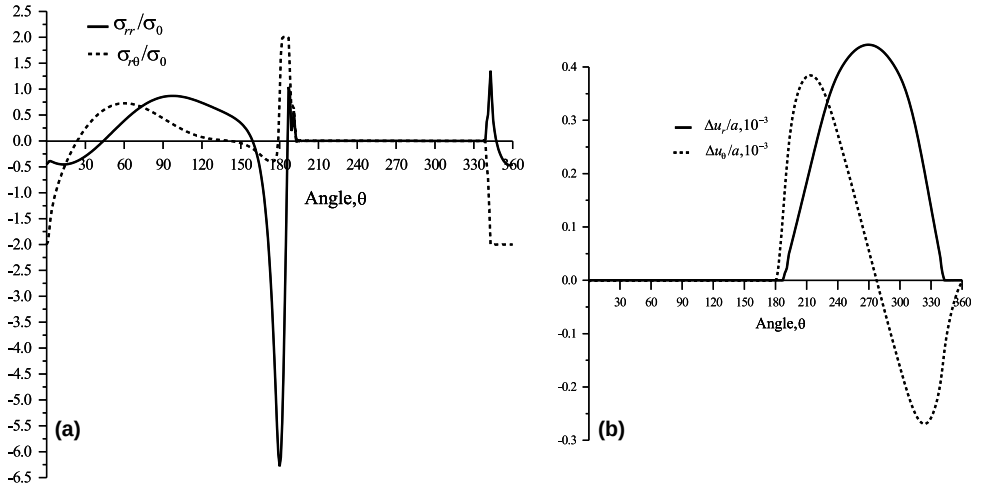

Fig. 21. Stresses (a) and displacement discontinuities (b) for inclusion 1 in Fig. 17 for $d/a = 1.01$.

example, therefore, the inclusion is loosened by either debonding or slippage over an arc of approximately 162°, or 45% of its periphery.

The zones of slip and separation are even more pronounced when the inclusions are closer together. This can be seen from Figs. 20 and 21, which show the distributions of stress and displacement discontinuity along the boundary of inclusion 1 for $d/a = 1.05$ and 1.01. (The numerical solutions for these cases required 72 and 85 iterations, respectively.) The proximity of the inclusions causes the zones of slip and separation to spread until, for the most severe case examined, $d/a = 1.01$, the inclusion is loosened over its entire lower half. It should also be noticed, however, that the radial compression in the vicinity of $\theta = 180°$ increases rapidly as $d/a \to 1$. If frictional effects were being considered, the increased compression would serve to inhibit slip over some parts of the interface.

6. Concluding remarks

The numerical procedure presented in this paper is designed to model the evolution of interfacial damage for multiple, randomly distributed circular elastic inclusions in an elastic plane. Damage is characterized by the occurrence of displacement discontinuities along the inclusion/matrix interfaces, because displacement discontinuities physically represent localized slip and/or separation of these interfaces.

For problems in which damage occurs, we have found that relatively large numbers of terms are required in the truncated Fourier series representations of the interface parameters, even when the inclusions are not close to touching. Therefore, rather than attempting to determine the optimal numbers of terms in the Fourier series during the iteration process—as can conveniently be done when the inclusions are perfectly bonded (Crouch and Mogilevskaya, 2003)—in the examples considered to date we have simply fixed the numbers of terms at the outset, taking the value of N_k large enough for each inclusion k to model any damage that might occur.

We have not looked carefully at the efficiency of our algorithm, and this is an issue that clearly needs attention. The rate of convergence of the iteration process is slow when two or more inclusions are close to touching, and this difficulty is even more pronounced when damage occurs. The current algorithm relies on the use of an under-relaxation parameter to achieve convergence, and we are not aware of any theoretical guidance for selecting this parameter for non-linear problems. By trial, we have found that the value

$\omega = 0.5$ usually works satisfactorily, although it some cases it seems likely that the rate of convergence could be improved by dynamically adjusting ω during the iteration process. Additional work is required to support this tentative conclusion, however.

Longer term, we plan to refine the iterative procedure by using the fast multipole technique (Rokhlin, 1985; Greengard and Rokhlin, 1987; Carrier et al., 1988) to efficiently represent the far-field influences of groups of inclusions by means of Taylor expansions. A more critical consideration for now, however, is to seek ways of improving the performance of the iteration process for even a few closely spaced inclusions.

Appendix A. Displacements and stresses in the matrix

The displacements and stresses at an arbitrary point $(x, y) = (\xi_x, \xi_y)$ in the matrix can be expressed as the initial values of these quantities due to the stresses at infinity plus the contributions from the K circular holes. As in our previous work (Crouch and Mogilevskaya, 2003), we represent the latter in terms of local polar coordinates r_k, χ_k originating at the center of the kth hole. In addition, we define a dimensionless parameter $\rho_k = r_k/R_k$, where R_k is the radius of the hole. For a point in the matrix we have that $\rho_k \geqslant 1$.

Using these definitions, the displacements at point $(x, y) = (\xi_x, \xi_y)$ are

$$
\begin{aligned}
u_x(\xi_x,\xi_y) = {} & \frac{1}{4\mu}[k_1\sigma^\infty_{xx} - (1-k_2)\sigma^\infty_{yy}]\xi_x + \frac{1}{2\mu}\sigma^\infty_{xy}\xi_y \\
& + \frac{1}{2k_1}\sum_{k=1}^{K}\left(\frac{1}{2\rho_k}\left[\left\{\frac{-R_k}{2\mu}(a_{1k}(t_x)+b_{1k}(t_y)) + a_{1k}(u_x) + b_{1k}(u_y)\right\}\cos\chi_k\right.\right. \\
& \left. + \{a_{1k}(u_y) - b_{1k}(u_x)\}\sin\chi_k\right] + \sum_{n=1}^{N_k}\frac{1}{\rho_k^n}\left[\left\{\frac{R_k}{2\mu n}k_3 a_{nk}(t_x) + k_1 a_{nk}(u_x) - k_2 b_{nk}(u_y)\right\}\cos n\chi_k\right. \\
& + \left\{\frac{R_k}{2\mu n}k_3 b_{nk}(t_x) + k_1 b_{nk}(u_x) + k_2 a_{nk}(u_y)\right\}\sin n\chi_k \\
& \left.\left. + \frac{1}{2}\left(1-\frac{1}{\rho_k^2}\right)\frac{R_k}{2\mu}\{D_{nk}\cos(n+2)\chi_k + S_{nk}\sin(n+2)\chi_k\}\right]\right) \\
u_y(\xi_x,\xi_y) = {} & \frac{1}{2\mu}\sigma^\infty_{xy}\xi_x + \frac{1}{4\mu}[-(1-k_2)\sigma^\infty_{xx} + k_1\sigma^\infty_{yy}]\xi_y \\
& + \frac{1}{2k_1}\sum_{k=1}^{K}\left(\frac{1}{2\rho_k}\left[-\{a_{1k}(u_y) - b_{1k}(u_x)\}\cos\chi_k\right.\right. \\
& \left. - \left\{\frac{R_k}{2\mu}(a_{1k}(t_x)+b_{1k}(t_y)) - a_{1k}(u_x) - b_{1k}(u_y)\right\}\sin\chi_k\right] \\
& + \frac{1}{2k_1}\sum_{n=1}^{N_k}\frac{1}{\rho_k^n}\left[\left\{\frac{R_k}{2\mu n}k_3 a_{nk}(t_y) + k_1 a_{nk}(u_y) + k_2 b_{nk}(u_x)\right\}\cos n\chi_k\right. \\
& + \left\{\frac{R_k}{2\mu n}k_3 b_{nk}(t_y) + k_1 b_{nk}(u_y) - k_2 a_{nk}(u_x)\right\}\sin n\chi_k \\
& \left.\left. - \frac{1}{2}\left(1-\frac{1}{\rho_k^2}\right)\frac{R_k}{2\mu}\{S_{nk}\cos(n+2)\chi_k - D_{nk}\sin(n+2)\chi_k\}\right]\right)
\end{aligned}
\tag{A.1}
$$

where

$$S_{nk} = a_{nk}(t_y) + b_{nk}(t_x) + \frac{2\mu n}{R_k}(a_{nk}(u_y) + b_{nk}(u_x))$$
$$D_{nk} = a_{nk}(t_x) - b_{nk}(t_y) + \frac{2\mu n}{R_k}(a_{nk}(u_x) - b_{nk}(u_y)) \tag{A.2}$$

Notice that the Fourier coefficients $a_{0k}(u_x)$ and $a_{0k}(u_y)$ do not appear in Eq. (A.1). As explained in Crouch and Mogilevskaya (2003), the values of these quantities are arbitrary insofar as calculation of the displacements at the point $(x, y) = (\xi_x, \xi_y)$ is concerned.

The stresses associated with displacements (A.1) are

$$\begin{aligned}
\sigma_{xx}(\xi_x,\xi_y) = \sigma^{\infty}_{xx} &+ \frac{1}{2k_1}\sum_{k=1}^{K}\left(\frac{1}{2\rho_k^2}\left[\left\{a_{1k}(t_x) + b_{1k}(t_y) - \frac{2\mu}{R_k}(a_{1k}(u_x) + b_{1k}(u_y))\right\}\cos 2\chi_k\right.\right.\\
&\left. - \frac{2\mu}{R_k}\{a_{1k}(u_y) - b_{1k}(u_x)\}\sin 2\chi_k\right] - \sum_{n=1}^{N_k}\frac{1}{\rho_k^{n+1}}\left[\left\{(1+k_1)a_{nk}(t_x) - (1-k_2)b_{nk}(t_y)\right.\right.\\
&\left. + \frac{2\mu n}{R_k}(2a_{nk}(u_x) - b_{nk}(u_y))\right\}\cos(n+1)\chi_k\\
&+ \left\{(1-k_2)a_{nk}(t_y) + (1+k_1)b_{nk}(t_x) + \frac{2\mu n}{R_k}(a_{nk}(u_y) + 2b_{nk}(u_x))\right\}\sin(n+1)\chi_k\\
&- D_{nk}\left\{\cos\chi_k\cos(n+2)\chi_k - \frac{(n+2)}{2}\left(1 - \frac{1}{\rho_k^2}\right)\cos(n+3)\chi_k\right\}\\
&\left.\left. - S_{nk}\left\{\cos\chi_k\sin(n+2)\chi_k - \frac{(n+2)}{2}\left(1 - \frac{1}{\rho_k^2}\right)\sin(n+3)\chi_k\right\}\right]\right)\\
\sigma_{yy}(\xi_x,\xi_y) = \sigma^{\infty}_{yy} &- \frac{1}{2k_1}\sum_{k=1}^{K}\left(\frac{1}{2\rho_k^2}\left[\left\{a_{1k}(t_x) + b_{1k}(t_y) - \frac{2\mu}{R_k}(a_{1k}(u_x) + b_{1k}(u_y))\right\}\cos 2\chi_k\right.\right.\\
&\left. - \frac{2\mu}{R_k}\{a_{1k}(u_y) - b_{1k}(u_x)\}\sin 2\chi_k\right]\\
&- \sum_{n=1}^{N_k}\frac{1}{\rho_k^{n+1}}\left[\left\{(1-k_2)a_{nk}(t_x) - (1+k_1)b_{nk}(t_y) + \frac{2\mu n}{R_k}(a_{nk}(u_x) - 2b_{nk}(u_y))\right\}\cos(n+1)\chi_k\right.\\
&+ \left\{(1+k_1)a_{n_k}(t_y) + (1-k_2)b_{n_k}(t_x) + \frac{2\mu n}{R_k}(2a_{nk}(u_y) + b_{nk}(u_x))\right\}\sin(n+1)\chi_k\\
&- D_{nk}\left\{\sin\chi_k\sin(n+2)\chi_k + \frac{(n+2)}{2}\left(1 - \frac{1}{\rho_k^2}\right)\cos(n+3)\chi_k\right\}\\
&\left.\left. + S_{nk}\left\{\sin\chi_k\cos(n+2)\chi_k - \frac{(n+2)}{2}\left(1 - \frac{1}{\rho_k^2}\right)\sin(n+3)\chi_k\right\}\right]\right)\\
\sigma_{xy}(\xi_x,\xi_y) = \sigma^{\infty}_{xy} &+ \frac{1}{4k_1}\sum_{k=1}^{K}\left(\frac{1}{\rho_k^2}\left[\frac{2\mu}{R_k}\{a_{1k}(u_y) - b_{1k}(u_x)\}\cos 2\chi_k\right.\right.\\
&\left. + \left\{a_{1k}(t_x) + b_{1k}(t_y) - \frac{2\mu}{R_k}(a_{1k}(u_x) + b_{1k}(u_y))\right\}\sin 2\chi_k\right]\\
&- \sum_{n=1}^{N_k}\frac{1}{\rho_k^{n+1}}\left[\left\{k_3(a_{nk}(t_y) - b_{nk}(t_x)) + \frac{2\mu n}{R_k}(a_{nk}(u_y) - b_{nk}(u_x))\right\}\cos(n+1)\chi_k\right.\\
&+ \left\{k_3(a_{nk}(t_x) + b_{nk}(t_y)) + \frac{2\mu n}{R_k}(a_{nk}(u_x) + b_{nk}(u_y))\right\}\sin(n+1)\chi_k\\
&\left.\left. + S_{nk}\left\{\left(1 - (n+2)\left(1 - \frac{1}{\rho_k^2}\right)\right)\cos(n+3)\chi_k\right\} - D_{nk}\left\{\left(1 - (n+2)\left(1 - \frac{1}{\rho_k^2}\right)\right)\sin(n+3)\chi_k\right\}\right]\right)
\end{aligned} \tag{A.3}$$

Appendix B. Displacements and stresses in an inclusion

The displacements and stresses at an arbitrary point $(x,y)=(\xi_x,\xi_y)$ within the kth inclusion can similarly be written in terms of local polar coordinates $\rho_k = r_k/R_k$, χ_k originating at the center of the inclusion. In this case, we have that $0 \leqslant \rho_k \leqslant 1$.

The displacements of the inclusion can be expressed in terms of the Fourier coefficients for the displacements only (cf. (A.1)):

$$
\begin{aligned}
u_x(\xi_x,\xi_y) &= \frac{1}{2}a'_{0k}(u_x) + \frac{1}{4\mu_k}[k_{1k}\sigma^{\infty}_{xx} - (1-k_{2k})\sigma^{\infty}_{yy}]\xi_x + \frac{1}{2\mu_k}\sigma^{\infty}_{xy}\xi_y \\
&\quad + \sum_{n=1}^{N_k}\rho_k^n\left[a'_{nk}(u_x)\cos n\chi_k + b'_{nk}(u_x)\sin n\chi_k\right] \\
&\quad + \frac{1}{2k_{3k}}\sum_{n=2}^{N_k} n(\rho_k^{n-2}-\rho_k^n)\left[(a'_{nk}(u_x)+b'_{nk}(u_y))\cos(n-2)\chi_k\right. \\
&\quad \left. -(a'_{nk}(u_y)-b'_{nk}(u_x))\sin(n-2)\chi_k\right] \\
u_y(\xi_x,\xi_y) &= \frac{1}{2}a'_{0k}(u_y) + \frac{1}{2\mu_k}\sigma^{\infty}_{xy}\xi_x + \frac{1}{4\mu_k}[-(1-k_{2k})\sigma^{\infty}_{xx} + k_{1k}\sigma^{\infty}_{yy}]\xi_y \\
&\quad + \sum_{n=1}^{N_k}\rho_k^n\left[a'_{nk}(u_y)\cos n\chi_k + b'_{nk}(u_y)\sin n\chi_k\right] \\
&\quad - \frac{1}{2k_{3k}}\sum_{n=2}^{N_k} n(\rho_k^{n-2}-\rho_k^n)\left[(a'_{nk}(u_y)-b'_{nk}(u_x))\cos(n-2)\chi_k\right. \\
&\quad \left. +(a'_{nk}(u_x)+b'_{nk}(u_y))\sin(n-2)\chi_k\right]
\end{aligned}
\tag{B.1}
$$

The coefficients $a'_{0k}(u_x)$ and $a'_{0k}(u_y)$ are needed in this case to account for possible translations of the inclusion.

The stresses associated with displacements (B.1) can be expressed in terms of the Fourier coefficients for the tractions, and do not directly depend on the elastic constants:

$$
\begin{aligned}
\sigma_{xx}(\xi_x,\xi_y) &= \sigma^{\infty}_{xx} - a_{1k}(t_x) - \rho_k(b_{2k}(t_x)-a_{2k}(t_y))\sin\chi_k \\
&\quad - \sum_{n=2}^{N_k}\rho_k^{n-1}[a_{nk}(t_x)\cos(n-1)\chi_k + b_{nk}(t_x)\sin(n-1)\chi_k] \\
&\quad + \sum_{n=3}^{N_k}\rho_k^{n-3}\left[(a_{nk}(t_x)+b_{nk}(t_y))\left\{\rho_k^2\sin\chi_k\sin(n-2)\chi_k - \frac{(n-2)}{2}(1-\rho_k^2)\cos(n-3)\chi_k\right\}\right. \\
&\quad \left. +(a_{nk}(t_y)-b_{nk}(t_x))\left\{\rho_k^2\sin\chi_k\cos(n-2)\chi_k + \frac{(n-2)}{2}(1-\rho_k^2)\sin(n-3)\chi_k\right\}\right] \\
\sigma_{yy}(\xi_x,\xi_y) &= \sigma^{\infty}_{yy} - b_{1k}(t_y) - \rho_k(a_{2k}(t_x)+b_{2k}(t_y))\cos\chi_k \\
&\quad - \sum_{n=2}^{N_k}\rho_k^{n-1}\left[b_{nk}(t_y)\cos(n-1)\chi_k - a_{nk}(t_y)\sin(n-1)\chi_k\right] \\
&\quad - \sum_{n=3}^{N_k}\rho_k^{n-3}\left[(a_{nk}(t_x)+b_{nk}(t_y))\left\{\rho_k^2\cos\chi_k\cos(n-2)\chi_k - \frac{(n-2)}{2}(1-\rho_k^2)\cos(n-3)\chi_k\right\}\right. \\
&\quad \left. +(a_{nk}(t_y)-b_{nk}(t_x))\left\{\rho_k^2\cos\chi_k\sin(n-2)\chi_k - \frac{(n-2)}{2}(1-\rho_k^2)\sin(n-3)\chi_k\right\}\right]
\end{aligned}
$$

$$\sigma_{xy}(\xi_x,\xi_y)=\sigma_{xy}^{\infty}-\frac{1}{2}(a_{1k}(t_y)+b_{1k}(t_x))-\rho_k[(a_{2k}(t_y)-b_{2k}(t_x))\cos\chi_k-(a_{2k}(t_x)+b_{2k}(t_y))\sin\chi_k]$$
$$-\sum_{n=2}^{N_k}\rho_k^{n-1}\left[b_{nk}(t_x)\cos(n-1)\chi_k+b_{nk}(t_y)\sin(n-1)\chi_k\right]$$
$$+\sum_{n=3}^{N_k}\rho_k^{n-3}\left[(a_{nk}(t_x)+b_{nk}(t_y))\left\{\rho_k^2\sin\chi_k\cos(n-2)\chi_k+\frac{(n-2)}{2}(1-\rho_k^2)\sin(n-3)\chi_k\right\}\right.$$
$$\left.-(a_{nk}(t_y)-b_{nk}(t_x))\left\{\rho_k^2\cos\chi_k\cos(n-2)\chi_k-\frac{(n-2)}{2}(1-\rho_k^2)\cos(n-3)\chi_k\right\}\right] \tag{B.2}$$

Appendix C. Determination of fourier coefficients by least squares

To determine the Fourier coefficients $a_{nj}^*(t_x)$, $b_{nj}^*(t_x)$, $a_{nj}^*(t_y)$, and $b_{nj}^*(t_y)$ associated with the adjusted trial traction changes t_x^* and t_y^* in (37), we apply the least squares methodology used by Barnes and Janković (1999) for an analogous problem in groundwater flow. In this approach, we select M_j uniformly spaced control points around the boundary of the jth inclusion, compute the adjusted trial tractions at these points due to the stresses at infinity as well as the influences of all of the other inclusions $k=1$ to K, $k\neq j$, and then minimize the following functions with respect to $a_{nj}^*(t_x)$, $b_{nj}^*(t_x)$, etc.:

$$\Lambda_x^2=\sum_{m=1}^{M_j}\left[\sum_{n=1}^{N_j}[a_{nj}^*(t_x)\cos n\theta_{mj}+b_{nj}^*(t_x)\sin n\theta_{mj}]-t_x^*(R_j,\theta_{mj})\right]^2$$
$$\Lambda_y^2=\sum_{m=1}^{M_j}\left[\sum_{n=1}^{N_j}[a_{nj}^*(t_y)\cos n\theta_{mj}+b_{nj}^*(t_y)\sin n\theta_{mj}]-t_y^*(R_j,\theta_{mj})\right]^2 \tag{C.1}$$

in which we assume $M_j\geqslant N_j$.

Successively differentiating the first one of (C.1) with respect to $a_{pj}^*(t_x)$ and $b_{pj}^*(t_x)$ and setting the resulting expressions equal to zero gives the following formulas:

$$\sum_{m=1}^{M_j}\left[\sum_{n=1}^{N_j}[a_{nj}^*(t_x)\cos n\theta_{mj}+b_{nj}^*(t_x)\sin n\theta_{mj}]-t_x^*(R_j,\theta_{mj})\right]\cos p\theta_{mj}=0$$
$$\sum_{m=1}^{M_j}\left[\sum_{n=1}^{N_j}[a_{nj}^*(t_x)\cos n\theta_{mj}+b_{nj}^*(t_x)\sin n\theta_{mj}]-t_x^*(R_j,\theta_{mj})\right]\sin p\theta_{mj}=0 \tag{C.2}$$

Similarly, differentiation of the second one of (C.1) with respect to $a_{pj}^*(t_y)$ and $b_{pj}^*(t_y)$ gives

$$\sum_{m=1}^{M_j}\left[\sum_{n=1}^{N_j}[a_{nj}^*(t_y)\cos n\theta_{mj}+b_{nj}^*(t_y)\sin n\theta_{mj}]-t_y^*(R_j,\theta_{mj})\right]\cos p\theta_{mj}=0$$
$$\sum_{m=1}^{M_j}\left[\sum_{n=1}^{N_j}[a_{nj}^*(t_y)\cos n\theta_{mj}+b_{nj}^*(t_y)\sin n\theta_{mj}]-t_y^*(R_j,\theta_{mj})\right]\sin p\theta_{mj}=0 \tag{C.3}$$

If the M_j control points are uniformly spaced around the boundary it can be shown that

$$\sum_{m=1}^{M_j} \cos n\theta_{mj} \sin p\theta_{mj} = \sum_{m=1}^{M_j} \sin n\theta_{mj} \cos p\theta_{mj} = 0 \tag{C.4}$$

and

$$\sum_{m=1}^{M_j} \cos n\theta_{mj} \cos p\theta_{mj} = \sum_{m=1}^{M_j} \sin n\theta_{mj} \sin p\theta_{mj} = \begin{cases} \frac{M_j}{2}; & p = n \\ 0; & p \neq n \end{cases} \tag{C.5}$$

for p and $n = 1$ to N_j, and hence

$$\begin{aligned} a^*_{nj}(t_x) &= \frac{2}{M_j} \sum_{m=1}^{M_j} t^*_x(R_j, \theta_{mj}) \cos n\theta_{mj}; \quad b^*_{nj}(t_x) = \frac{2}{M_j} \sum_{m=1}^{M_j} t^*_x(R_j, \theta_{mj}) \sin n\theta_{mj} \\ a^*_{nj}(t_y) &= \frac{2}{M_j} \sum_{m=1}^{M_j} t^*_y(R_j, \theta_{mj}) \cos n\theta_{mj}; \quad b^*_{nj}(t_y) = \frac{2}{M_j} \sum_{m=1}^{M_j} t^*_y(R_j, \theta_{mj}) \sin n\theta_{mj} \end{aligned} \tag{C.6}$$

References

Aboudi, J., 1987. Damage in composites—modeling of imperfect bonding. Composites Science and Technology 28, 103–128.

Achenbach, J.D., Zhu, H., 1989. Effect of interfacial zone on mechanical behavior and failure of fiber-reinforced composites. Journal of the Mechanics and Physics of Solids 37, 381–393.

Achenbach, J.D., Zhu, H., 1990. Effect of interphases on micro and macromechanical behavior of hexagonal-array fiber composites. ASME Journal of Applied Mechanics 57, 956–963.

Al-Ostaz, A., Jasiuk, I., 1996. The influence of interface and arrangement of inclusions on local stresses in composite materials. Acta Materialia 45, 4131–4143.

Barenblatt, G.I., 1962. The mathematical theory of equilibrium cracks in brittle fracture. Advances in Applied Mechanics 7, 55–129.

Barnes, R.J., Janković, I., 1999. Two-dimensional flow through large numbers of circular inhomogeneities. Journal of Hydrology 226, 204–210.

Bažant, Z.P., Planas, J., 1998. Fracture and Size Effect in Concrete and Other Quasibrittle Materials. CRC Press, Boca Raton.

Benveniste, Y., 1985. The effective mechanical behavior of composite materials with imperfect contact between the constituents. Mechanics of Materials 4, 197–208.

Benveniste, Y., Miloh, T., 2001. Imperfect soft and stiff interfaces in two-dimensional elasticity. Mechanics of Materials 33, 309–323.

Carrier, J., Greengard, L., Rokhlin, V., 1988. A fast adaptive multipole algorithm for particle simulations. SIAM Journal on Scientific and Statistical Computation 9, 669–686.

Chao, R., Laws, N., 1997. The fiber–matrix interface crack. ASME Journal of Applied Mechanics 64, 992–999.

Churchill, R.V., 1963. Fourier Series and Boundary Value Problems. McGraw-Hill, New York.

Crouch, S.L., Mogilevskaya, S.G., 2003. On the use of Somigliana's formula and Fourier series for elasticity problems with circular boundaries. International Journal for Numerical Methods in Engineering 58, 537–578.

Dugdale, D.S., 1960. Yielding of steel sheets containing slits. Journal of the Mechanics and Physics of Solids 8, 100–104.

Gao, Z., 1995. A circular inclusion with imperfect interface: Eshelby's tensor and related problems. ASME Journal of Applied Mechanics 62, 860–866.

Golub, G.H., Van Loan, C.F., 1996. Matrix Computation. J. Hopkins University Press, Baltimore.

Greengard, L., Rokhlin, V., 1987. A fast algorithm for particle simulations. Journal of Computational Physics 73, 325–348.

Hashin, Z., 1990. Thermoelastic properties of fiber composites with imperfect interface. Mechanics of Materials 8, 333–348.

Hashin, Z., 1991. The spherical inclusion with imperfect interface. ASME Journal of Applied Mechanics 58, 444–449.

Hussain, M.A., Pu, S.L., 1971. Slip phenomenon for a circular inclusion. ASME Journal of Applied Mechanics 38, 627–633.

Jerri, A.J., 1998. The Gibbs Phenomenon in Fourier Analysis, Splines and Wavelet Approximations. Kluwer Academic Publishers, Dordrecht, The Netherlands.

Ju, J.W., Lee, H.K., 2001. A micromechanical damage model for effective elastoplastic behavior of partially debonded ductile matrix composites. International Journal of Solids and Structures 38, 6307–6332.

Lagache, M., Agbossou, A., Pastor, J., 1994. Role of interphase on the elastic behavior of composite materials: Theoretical and experimental analysis. Journal of Composite Materials 28, 1140–1157.

Lanczos, C., 1966. Discourse on Fourier Series. Oliver and Boyd, Edinburgh.

Liu, Y.J., Xu, N., Luo, J.F., 2000. Modeling of interphases in fiber-reinforced composites under transverse loading using the boundary element method. ASME Journal of Applied Mechanics 67, 41–49.

Mogilevskaya, S.G., Crouch, S.L., 2002. A Galerkin boundary integral method for multiple circular elastic inclusions with homogeneously imperfect interfaces. International Journal of Solids and Structures 39, 4723–4746, Erratum 2003; 40:1335.

Mogilevskaya, S.G., Crouch, S.L., 2003. A Galerkin boundary integral method for multiple circular elastic inclusions with uniform interphase layers. International Journal of Solids and Structures 41, 1285–1311.

Nassehi, V., Dhillon, J., Mascia, L., 1993. Finite element simulation of the micromechanics of interlayered polymer/fibre composites: A study of the interactions between the reinforcing phases. Composites Science and Technology 47, 349–358.

Noble, B., Hussain, M.A., 1969. Exact solution of certain dual series for indentation and inclusion problems. International Journal of Engineering Science 7, 1149–1161.

Rokhlin, V., 1985. Rapid solution of integral equations of classical potential theory. Journal of Computational Physics 60, 187–207.

Ru, C.Q., 1998. A circular inclusion with circumferentially inhomogeneous sliding interface in plane elastostatics. ASME Journal of Applied Mechanics 65, 30–38.

Sheremet'ev, M.P., 1952. The elastic equilibrium of an infinite plate with an inserted absolutely rigid or elastic disk. PMM 16, 437–448 (in Russian).

Stippes, M., Wilson Jr., H.B., Krull, F.N., 1962. A contact stress problem for a smooth disk in an infinite plate. Proceedings of the Fourth US National Congress of Applied Mechanics, 799–806.

Sudak, L.J., Ru, C.Q., Schiavone, P., Mioduchowski, A., 1999. A circular inclusion with inhomogeneously imperfect interface in plane elasticity. Journal of Elasticity 55, 19–41.

Sun, L.Z., Ju, J.W., Liu, H.T., 2003. Elastoplastic modeling of metal matrix composites with evolutionary particle debonding. Mechanics of Materials 35, 559–569.

Toya, M., 1974. A crack along the interface of a circular inclusion embedded in an infinite solid. Journal of the Mechanics and Physics of Solids 22, 325–348.

Varga, R.S., 2000. Matrix Iterative Analysis, second ed. Springer, New York.

Wacker, G., Bledzki, A.K., Chate, A., 1998. Effect of interphase on the transverse Young's modulus of glass/epoxy composites. Composites 29, 619–626.

Zhao, Y.H., Weng, G.J., 1997. Transversely isotropic moduli of two partially debonded composites. International Journal of Solids and Structures 34, 493–507.

Zhu, H., Achenbach, J.D., 1991. Radial matrix cracking and interphase failure in transversely loaded fiber composites. Mechanics of Materials 11, 347–356.